NASA TECHNICAL NOTE

NASA TN D-3501

C. 1

NASA TN D-3501

FLUTTER STUDIES OF SIMPLIFIED COMPONENT MODELS OF A VARIABLE-SWEEP-WING AIRPLANE AT MACH NUMBERS UP TO 3.0

by Maynard C. Sandford, Charles L. Ruhlin, and Irving Abel

Langley Research Center
Langley Station, Hampton, Va.

NATIONAL AERONAUTICS AND SPACE ADMINISTRATION • WASHINGTON, D. C. • JULY 1966

FLUTTER STUDIES OF SIMPLIFIED COMPONENT MODELS OF A VARIABLE-SWEEP-WING AIRPLANE AT MACH NUMBERS UP TO 3.0

By Maynard C. Sandford, Charles L. Ruhlin,
and Irving Abel

Langley Research Center
Langley Station, Hampton, Va.

NATIONAL AERONAUTICS AND SPACE ADMINISTRATION

For sale by the Clearinghouse for Federal Scientific and Technical Information
Springfield, Virginia 22151 – Price $2.00

FLUTTER STUDIES OF SIMPLIFIED COMPONENT MODELS OF A VARIABLE-SWEEP-WING AIRPLANE AT MACH NUMBERS UP TO 3.0

By Maynard C. Sandford, Charles L. Ruhlin,
and Irving Abel
Langley Research Center

SUMMARY

Wind-tunnel flutter trend studies of simplified component models of a variable-sweep-wing airplane have been conducted at Mach numbers from about 0.6 to 3.0. The model configurations investigated included an aspect-ratio-9 wing at sweepback angles of 16°, 39°, and 73°, an aspect-ratio-8 wing at a sweepback angle of 16°, an all-movable horizontal tail which had a 20° sweptback pitch axis, and a vertical tail (including a rudder) with and without a tip weight (radome). The model flutter panels consisted of tapered plates cut to the desired planform with wedge-shaped leading and trailing edges. All models of a given component approximated the fundamental vibration modal characteristics of the respective airplane component.

The wing flutter-speed boundary shapes are typical of those of comparable planforms. At subsonic Mach numbers, increasing the sweep angle of the wing sizably increased the dynamic pressure required for flutter. For the lower sweep angles, the transonic region is the most critical flutterwise; hence, suitable flight programing of the wing sweep angle could minimize structural requirements for flutter prevention. The flutter speeds for the lower sweep angles are very sensitive to mass-density-ratio effects and, in order to interpret accurately data from models of the present type, mass-density-ratio effects should be thoroughly explored. The wing with an aspect ratio of 9 is more susceptible to flutter than the wing with an aspect ratio of 8.

The flutter-speed boundary for the horizontal tail is relatively flat at the low supersonic Mach numbers, with the boundary level only slightly higher than the transonic dip; thus, for a constant-altitude flight profile the low supersonic speed region is the most critical for this component. Simplified supersonic flutter calculations indicate that the experimental trends appear to be reasonable. The flutter-speed boundary for the vertical tail with tip weight (radome) is typical of those for surfaces of moderate sweep and aspect ratio. The removal of the tip weight only slightly increased the dynamic pressure required for flutter at near sonic speeds. The rudder rotational stiffness is indicated to be a significant parameter affecting the flutter speed of this component.

INTRODUCTION

The structural design of high-performance airplanes is often significantly influenced by flutter clearance requirements so that the pertinent flutter boundaries must be accurately known early in the design process if sizable weight penalties and costly fixes are to be avoided. Generally, flutter requirements are established in several stages of combined analyses and experiments. (For example, see ref. 1.) Preliminary flutter requirements for the main aerodynamic surfaces are determined from subsonic flutter calculations and from an estimate of the transonic flutter characteristics based on experimental data because analytical methods are least reliable in the transonic range. From these preliminary estimates, flutter problem areas are defined and, as the airplane design evolves, further analyses and experiments with more exactly scaled models are made to explore these problem areas and to optimize the design flutterwise. Finally, as the airplane design becomes fixed, detailed analyses and sophisticated flutter models (such as complete airplane flutter models) are used to demonstrate flutter clearances and to provide guidance for flight flutter tests.

In order to provide experimental data for use in establishing preliminary flutter requirements for a variable-sweep-wing airplane, flutter studies of simplified models of the wing, horizontal tail, and vertical tail of this airplane were conducted at Mach numbers from about 0.6 up to 3.0. These models were similar in construction to those used previously for establishing transonic flutter trends (ref. 2), and were simplified tapered-plate models which scaled only the planform. However, all models of a given component approximated the successive frequency ratios and the fundamental vibration modal characteristics for the respective airplane component. Wing configurations investigated included an aspect-ratio-9 wing at sweepback angles of 16°, 39°, and 73° and an aspect-ratio-8 wing at a sweepback angle of 16°. The all-movable horizontal-tail models included simulation of the pitch degree of freedom about an axis swept back 20°. The vertical-tail models were provided with a simulated rudder and were investigated with and without a heavy weight (radome) at the tip.

Presented herein are the results of the experimental flutter studies of the simplified component models. As an aid in the interpretation of the wing results, mass-density-ratio effects on the experimental flutter trends were examined. Also included in this report are the results of a brief theoretical analysis of the supersonic flutter characteristics of a horizontal-tail model. The transonic flutter tests were conducted in the Langley 26-inch transonic blowdown tunnel, and the supersonic tests were made in the Langley 20-inch variable supersonic tunnel and in the Langley Unitary Plan wind tunnel.

SYMBOLS

Measurements for this investigation were taken in the U.S. Customary System of Units. Equivalent values are indicated herein in the International System (SI) in the interest of promoting use of this system in future NASA reports. Details concerning the use of SI, together with physical constants and conversion factors, are given in reference 3.

b one-half mean aerodynamic chord, ft (m)

c streamwise chord, ft (m)

f flutter frequency, cps

f_i natural frequency of ith vibration mode, cps

f_r reference frequency: $f_r = f_3$ for wings and vertical tail with tip weight, $f_r = f_2$ for vertical tail without tip weight, $f_r = f_1$ for horizontal tail, cps

I mass moment of inertia of horizontal tail about horizontal-tail pivot axis, slug-ft^2 (kg-m^2)

I_{tb} mass moment of inertia of horizontal-tail torque bar about horizontal-tail pivot axis, slug-ft^2 (kg-m^2)

K rotational spring constant of horizontal tail about horizontal-tail pivot axis, ft-lb/rad (m-N/rad)

M Mach number

m_h total mass of horizontal tail, slugs (kg)

m_v total mass of vertical tail (including rudder) and tip weight when present, slugs (kg)

m_w total mass of movable wing, slugs (kg)

q dynamic pressure, lb/sq ft (kN/m^2)

q_{adj} — dynamic pressure at flutter adjusted to a selected reference stiffness level for similar planform models, lb/sq ft (kN/m^2)

$q_{min\Lambda}$ — dynamic pressure at flutter for wing minimum sweepback angle, lb/sq ft (kN/m^2)

t — model thickness, ft (m)

V — free-stream velocity, ft/sec (m/s)

v_h — volume of a conical frustum surrounding horizontal tail having exposed root chord as base diameter, tip chord as upper diameter, and exposed semispan as height, cu ft (m^3)

v_v — volume of a conical frustum surrounding vertical tail having exposed root chord as base diameter, tip chord as upper diameter, and exposed semispan as height, cu ft (m^3)

v_w — volume of a conical frustum surrounding movable wing model at $\Lambda = 16^o$ with streamwise chord at pivot as base diameter, tip chord as upper diameter, and spanwise distance from pivot to tip as height, cu ft (m^3)

Λ — leading-edge sweepback angle, deg

μ — mass-density ratio, $\frac{m_n}{\rho v_n}$ (where $n = h$, v, or w)

ρ — air density, slugs/cu ft (kg/m^3)

ω_i,ω_r — circular frequency, $2\pi f_i$ and $2\pi f_r$, respectively, rad/sec

MODELS

General Description

Semispan simplified models of the components of a variable-sweep-wing airplane were used in this investigation. Model properties are given in tables I to IV and in figure 1. Photographs of the models are presented in figure 2. The models of the wing (1/39-size), horizontal tail (1/21-size), and vertical tail (1/19-size) were tapered plates with wedge-shaped leading and trailing edges. The models simulated geometrically only planform shapes, and no attempt was made to scale elastic or mass properties. In order to obtain various stiffness levels for the models of the same component, the models were constructed with different basic thickness-chord ratios. However, all models of a given component, including those of different stiffness levels, did approximate the successive frequency ratios and the fundamental vibration modal characteristics of the respective airplane component. It is believed that this agreement in the vibration modes exists because each model was constructed to maintain the same thickness-chord ratio over the entire span.

Model Designation

Each model used in the investigation is identified by a coded designation. The first item in the designation is the letter W, H, or V and represents the wing, the horizontal-tail, or the vertical-tail component, respectively. The second item is a digit and represents a stiffness level for a given component (increasing numbers represent increasing stiffnesses). The third item, when given, is separated from the other two items by a dash and is a number that identifies the various models of a given stiffness level. For example, the designation W2-1 represents wing model 1 of stiffness level 2. (See table III.) An exception to this code is the second item in the horizontal-tail-model designation, which is composed of both a digit and a letter. The additional letter (either A, B, C, or D) is used to identify the pitch spring. (See table II(c).)

Construction

The models were constructed of aluminum alloy chemically etched to the desired thickness. The variable-sweep-wing joint was simulated by a simple pivot joint which restrained the movable wing panel at the selected sweep angle by tightening the threaded pivot pin and thereby producing a large friction force between the fixed-wing inner faces and a locally raised portion of the movable wing (fig. 2(a)). A small tapered pin was also used to lock the wing in position. The all-movable horizontal-tail pitch mechanism consisted of a steel torque shaft retained by two ball bearings in the mounting block and connected to an interchangeable steel rectangular torsion spring (fig. 2(b)). The vertical tail was cantilevered and the rudder was formed simply by cutting a portion of the overall planform shape. By not completely severing the rudder root leading edge, an effective rudder rotational spring was formed (figs. 1(c) and 2(c)). Rudder hinges were made of either nylon cord or brass flexures. A lead weight fastened at the tip and enclosed by a streamline balsa fairing simulated a radome.

Instrumentation

Model instrumentation consisted of wire strain gages oriented to indicate deflections in bending and torsion.

Physical Properties

Stiffness and mass properties of the models are given in table II and measured vibration properties are presented in tables III and IV and in figure 3. The thickness-chord ratios given in table II are a measure of the stiffness of the models. The fixed inboard wing section, which included the wing pivot, was relatively rigid and the wing frequency was invariant with sweepback angle. The desired horizontal-tail vibration frequencies were obtained through various combinations of model stiffness and pitch-spring stiffness. A concentrated mass, representing a radome, was located at the tip of the vertical tail for most of the flutter tests.

TEST APPARATUS AND TECHNIQUE

The investigation was conducted in the Langley 26-inch transonic blowdown tunnel (TBT), in the Langley 20-inch variable supersonic tunnel (VST), and in the Langley Unitary Plan wind tunnel (UPWT). The supersonic tests were made initially in the VST; however, the loss of several models due to the large starting loads necessitated completion of the supersonic tests in the UPWT, which possesses less severe starting conditions. The TBT has a slotted, 26-inch (66-cm) octagonal test section and is capable of operation at stagnation pressures up to 75 pounds per square inch (517 kN/m^2) at Mach numbers up to about 1.4. The VST is a flexible-wall blowdown tunnel having a 20-inch (51-cm) square test section and is capable of operation at stagnation pressures up to 125 pounds per square inch (861 kN/m^2) at Mach numbers from about 1.8 to 4.5. The UPWT is a continuous-flow variable pressure and variable Mach number tunnel with a 4-foot (1.22-m) square test section. For the low Mach number test section of the UPWT, one of its normal operating modes allows operation at stagnation pressures up to 34 pounds per square inch (234 kN/m^2) at a Mach number of 1.6 and up to 47 pounds per square inch (324 kN/m^2) at a Mach number of 2.16.

The models tested in the TBT were mounted on a 3-inch-diameter (7.6-cm) fuselage-sting which extended forward into the low-speed region of the tunnel in order to eliminate the formation of a bow shock wave. The sting was located about 5 inches (12.7 cm) from the tunnel center line. The models tested in the VST were mounted on a streamline fairing which extended about 3 inches (7.6 cm) from the tunnel wall to avoid boundary-layer interference. The UPWT models were mounted flush to a splitter plate mounted outside the boundary layer of the tunnel.

The tunnel stagnation pressure, stagnation temperature, test-section static pressure, and model strain-gage signals were continuously recorded on a direct readout recorder. Visual records of the model motion at flutter were obtained by use of high-speed motion-picture cameras.

Briefly, the test procedure consisted of establishing a test Mach number either by setting a given orifice (in the TBT) or by properly adjusting tunnel walls (in the VST and UPWT). Next the stagnation pressure was increased to a desired maximum value or until flutter was encountered, at which time the tunnel was shut down in hopes of avoiding model damage. This procedure was repeated for all desired Mach numbers up to 1.4, 3.0, or 2.16 depending on the tunnel in which the test was conducted. An additional mode of operation in the TBT was to vary the orifice plate (so that the test-section Mach number could be slowly decreased) at a constant stagnation pressure and thereby establish flutter boundaries in regions not easily obtained in the normal operational mode.

PRESENTATION OF RESULTS

The experimental results of the present investigation are compiled in table V and some of the experimental and analytical results are presented in figures 4 to 12. The basic experimental data are presented as variations with Mach number of the flutter-speed index $\left(\frac{V}{b\omega_r\sqrt{\mu}}\right)$, of the flutter-frequency ratio (f/f_r), and of the mass-density ratio (μ). In calculating the mass-density ratios for the various aspect-ratio-9 wings, the volume for the wing at a sweepback angle of 16° was used; hence, for the same wing mass and air density, the mass-density-ratio values are invariant with sweep angle. The basic data are given for the wings in figure 4, for the horizontal tail in figure 10, and for the vertical tail in figure 12. The flutter-speed boundaries shown as solid-line curves in these figures are those considered most representative for each component. The parts of the boundaries shown with dotted lines are regarded as questionable and are discussed in the following sections. As an indication of the vibration modes involved in the flutter, the range of the model frequency ratios is included on the ordinates of the flutter-frequency-ratio plots.

Additional plots of the wing data were made to establish a mass-ratio correction to the flutter-speed index for the aspect-ratio-9 wing at sweepback angles of 16° and 39° (figs. 5 to 7), to show the effect of varying sweepback angle at subsonic speeds (fig. 8), and to compare the results for the aspect-ratio-9 and aspect-ratio-8 wings (fig. 9). The results of the supersonic flutter calculations for the horizontal-tail models are given in figure 11.

DISCUSSION OF RESULTS

Wings

In general, the flutter-speed boundaries for the present wing configurations (fig. 4) are typical of those for similar planforms over the Mach number range investigated (i.e., the flutter boundary shape is relatively flat at subsonic speeds, dips in the transonic region, and rises to a substantially higher level at supersonic speeds). Unusual dips in flutter speed for the aspect-ratio-9 wing at sweepback angles of 16° and 39° were obtained over a relatively narrow range of Mach numbers near 1.07 (indicated by dotted lines in figs. 4(a) and (b)). However, because these dips occur in the Mach number range where shock waves may be reflecting back on the model and because flutter boundaries for similar planforms do not indicate comparable results, these particular dips are regarded as very questionable and are not considered to be characteristic of these two wing planforms.

The flutter modes for the aspect-ratio-9 wing at the lower sweep angles (figs. 4(a) and (b)) were characterized by a sudden change in the flutter mode near sonic speed. At subsonic and transonic speeds, the models fluttered with large tip amplitudes; whereas, at supersonic speeds, they fluttered with small tip amplitudes. The flutter mode of the aspect-ratio-8 wing at 16° sweep (fig. 4(d)) was nearly the same as that for the 16° swept aspect-ratio-9 wing over the limited speed range investigated. At the 73° sweepback angle, the aspect-ratio-9 wing fluttered (fig. 4(c)) in a limited amplitude mode which had a shape very similar to the second bending natural vibration mode and which did not vary appreciably with Mach number.

Although the overall shapes of the flutter-speed boundaries for the present wings were considered typical, the transonic dips in flutter speed for the lower wing sweep angles were unusually large and indicated a reduction in flutter speed of about 25, 23, and 15 percent for the 16° and 39° swept aspect-ratio-9 wing and the 16° swept aspect-ratio-8 wing, respectively. In addition, the scatter in the subsonic data for the 16° and 39° swept wings (figs. 4(a), (b), and (d)), rather than being random in nature, indicated possible distinct boundaries for models of each different stiffness level. These models had roughly similar frequency spectrums and vibration mode shapes, and all models of a given sweep angle fluttered in nearly the same flutter mode. However, distinct variations in the mass-density ratio (μ) at flutter could be traced for models of different stiffness levels over the Mach number range (figs. 4(a) and (b)). Since variations in the mass-density ratio may seriously affect the flutter-speed boundary (for example, see ref. 4), an attempt was made to reduce the experimental data to a constant mass-density ratio of 30, which was approximately the airplane sea-level value. This mass-density-ratio adjustment was restricted to the aspect-ratio-9 wing at 16° and 39° sweep because only a limited number of experimental points were available for the aspect-ratio-8 wing and because the scatter in the data for the 73° swept wing was apparently random.

The basic experimental data for the two wing planforms are plotted in figure 5 in terms of the flutter-speed index against experimental mass-density ratio. Since the effects of mass-density ratio are known to vary with Mach number (ref. 5), the data are plotted separately for subsonic Mach numbers ($M < 0.75$) and for transonic Mach numbers ($0.75 < M < 0.90$). The general trends obtained are shown by curves drawn through a rough mean of the experimental points, and these trend curves are normalized by the flutter-speed index at a mass-density ratio of 30 and replotted at the top of figure 5. In general, these trends agree qualitatively with those obtained in other experimental and analytical flutter investigations (refs. 5 and 6).

Figure 6 shows the experimental transonic flutter points which have been adjusted to a mass-density ratio of 30 based on the normalized curves of figure 5. For data points at Mach numbers greater than 0.9, the adjustment was made by using the transonic trends ($0.75 < M < 0.9$), and is considered a conservative approximation since flutter-speed calculations have shown that the effect of mass-density ratio becomes greater at the higher Mach numbers (ref. 5). It can be seen (fig. 6) that the scatter in the experimental data is substantially reduced. Although the subsonic level of the flutter-speed index is not appreciably affected, the transonic dip in flutter speed for the 16° swept wing and the 39° swept wing is reduced to about 7 and 3 percent, respectively, from the comparable unadjusted values of about 25 and 23 percent, respectively. The magnitude of this mass-density-ratio correction can be better appreciated by comparing the adjusted and unadjusted flutter boundaries in figure 7. It is apparent that the unadjusted flutter boundaries are very conservative, and in instances when flutter requirements established from experimental trend data seriously affect the airplane structural design, mass-density-ratio effects should be thoroughly explored.

Figure 7 also illustrates the effect of varying the sweepback angle on the flutter speed for the aspect-ratio-9 wing. At subsonic speeds, the flutter speeds for wing sweepback angles of 39° and 73° are about 12 and 66 percent, respectively, greater than that for the 16° swept wing. (These values are equivalent to an increase in dynamic pressure at flutter of 1.25 and 2.7.) Flutter requirements at transonic speeds could be greatly alleviated by suitable flight programing of the wing sweep angle. At Mach numbers above 2.35, the 73° swept wing had a lower flutter speed than the 39° swept wing. The effect of varying the sweepback angle at subsonic speeds for the aspect-ratio-9 wing is shown in figure 8 in terms of the variation with sweep angle of the flutter dynamic pressure normalized by the flutter dynamic pressure obtained for the minimum sweepback angle of the particular investigation. Included in figure 8 for comparison are the results of a previous investigation (ref. 7) of an untapered wing of aspect ratio 6.2 (based on semispan wing at 0° sweep). There was good agreement between the results for the two wings, with the variation in the flutter dynamic-pressure ratio for both wings more closely following the $1/\cos \Lambda$ relationship than the normal component of velocity relationship $1/\cos^2 \Lambda$.

The aspect-ratio-8 wing model, which was simply the aspect-ratio-9 wing with a tip section cut off, was investigated in order to verify that the higher aspect ratio wing was the more susceptible to flutter of the two planforms. The transonic flutter boundaries for the two wings at a sweepback angle of 16^{o} are presented in figure 9 in terms of a dynamic pressure adjusted to apply to a typical W4 model (model of stiffness level 4). These dynamic-pressure boundaries were determined by expanding the flutter-speed index boundaries (figs. 4(a) and (b)) to dynamic pressures as follows:

$$q_{adj} = \frac{1}{2}\left(\frac{V}{b\omega_3\sqrt{\mu}}\right)^2_{\text{Experimental curve}} \left(b\omega_3\sqrt{\frac{m_w}{v_w}}\right)^2_{\text{W4 model}}$$

However, these data have not been adjusted for differences in the experimental mass-density ratios. Since any mass-density-ratio adjustment would only be expected to reduce the size of the transonic dips for each planform, the aspect-ratio-9 wing would still flutter at dynamic pressures considerably lower than the aspect-ratio-8 wing and therefore, as was expected, is the more susceptible to flutter of the two planforms.

Horizontal Tails

The unusual amount of scatter in the experimental data obtained with the all-movable horizontal-tail models (fig. 10) at subsonic speeds ($M < 0.9$) and at the high supersonic speeds ($M \gtrsim 1.6$) made it difficult to define accurately a flutter-speed boundary in these regions. An attempt to adjust the experimental data to a constant mass-density ratio similar to the adjustment for the aspect-ratio-9 wing was made, but the results were not conclusive enough to establish an adjustment factor. Apparently this scatter is due not only to the variations in the experimental mass-density ratio but also to less obvious dissimilarities in model physical properties such as vibration frequency ratios and mode shapes. However, the difference in boundary level between the flutter speeds at $M \approx 1.2$ and the supersonic trend obtained in the UPWT (see fig. 10) is comparable to experimental results obtained in several previous investigations – for example, reference 5. Reference 5 demonstrates that the discrepancies in the flutter boundary levels obtained in different test facilities for the same planform models are the result of variations in the experimental mass-density ratios. With these considerations in mind, the flutter-speed boundary shown as the solid line in figure 10 is considered as more representative for this surface.

The flutter mode of the horizontal-tail models consisted of a distinct pitch mode combined with the bending mode, with the bending component varying from large amplitudes at transonic speeds to small amplitudes at supersonic speeds. At the subsonic and transonic Mach numbers, the subcritical behavior of the model was characterized by large bending amplitudes at the tip with the pitching motion progressively becoming more evident and sustained as the flutter boundary was approached. For some models, it was difficult to define the exact start of flutter, and large areas of doubtful flutter (i.e., low damping) were noted. (See fig. 10.)

The flutter-speed boundary for the all-movable horizontal tail exhibited an unexpected trend at low supersonic speeds (fig. 10). Unlike typical flutter-speed boundaries which rise rapidly with increasing Mach number in this speed range, a marked flatness was obtained in the present boundary, with the supersonic level just slightly higher then the transonic dip. However, similar experimental results for an all-movable control surface are reported in reference 8, and the present trends have been substantiated in subsequent tests (unpublished) with scaled dynamic-aeroelastic models of the present horizontal tail. The significance of this flat supersonic trend is that for a low-altitude flight profile which extends into the supersonic region, the critical region occurs at low supersonic Mach numbers.

In order to verify the supersonic trends for the horizontal-tail models, a simplified theoretical flutter analysis was made for an H2 model. The analysis employed aerodynamic forces evaluated from the Van Dyke quasi-steady second-order theory by the method outlined in reference 9. The first three coupled modes and frequency ratios of a typical H2 model (table IV(b)) were used, and the generalized masses for both main and off-diagonal terms of the dynamic matrix were included. The analyses covered a range of Mach numbers from 1.6 up to 2.5 and flow densities pertaining to mass-density ratios of 13.8, 27.5, 71.5, and 350. This range of mass-density ratios included all the experimental values. The calculated flutter-speed trends roughly follow the experimental trends (fig. 11) but the mass-density-ratio effects predicted by theory do not account completely for the difference in the flutter-speed level between results obtained in the VST and in the UPWT (fig. 10). However, the aerodynamic terms derived from second-order theory are known to be of questionable accuracy in the present Mach number range.

Vertical Tails

The flutter-speed boundary for the vertical tail with the tip weight (simulating a radome) was reasonably typical (fig. 12) with a transonic dip in flutter speed of about 12 percent and with the flutter speed increasing rapidly with Mach number at supersonic speeds. The flutter mode for the tip-weighted models was very similar to the second natural mode shape and consisted of rudder rotation and a relatively large bending motion of the fin area outboard of the tip node line (fig. 3(c)). Usually, flutter occurred suddenly and violently and after a few cycles of flutter motion the tip weight was shed, the outboard rudder hinges broken, and possibly the rudder lost. Since the tip weight had such a large influence on this flutter mode, limited tests were made to determine whether the flutter speed could be substantially raised by removing the tip weight. However, removing the tip weight only slightly increased the flutter dynamic pressure at near sonic speeds (table V(c)), and the models without tip weight fluttered in a mode that still involved considerable rudder rotation. Apparently the flutter mechanism was quite sensitive to the rudder rotation mode and probably the flutter dynamic pressures for both models could be raised by increasing the rudder rotational stiffness.

CONCLUSIONS

Wind-tunnel flutter trend studies of simplified component models of a variable-sweep-wing airplane have been conducted at Mach numbers from about 0.6 to 3.0. The model configurations included wings at leading-edge sweepback angles of 16°, 39°, and 73°, an all-movable horizontal tail, and a vertical tail.

Wing Models

The results obtained with the wing models are as follows:

1. The flutter boundary shapes were typical of those of similar planforms.

2. At subsonic Mach numbers, the wing at sweepback angles of 39° and 73° required a dynamic pressure for flutter 1.25 and 2.7 times greater than that for the 16° swept wing. For the lower sweepback angles, the transonic region was the most critical with regard to flutter. Hence, suitable flight programing of the wing sweep angles could minimize structural requirements for flutter prevention at transonic speeds.

3. The flutter speeds for the 16° and 39° wing sweep angles were quite sensitive to variations in mass-density ratio. Adjustment of the data to a constant mass-density-ratio value based on the present experimental trends considerably reduced the size of the transonic dip in the experimental flutter-speed boundaries. In order to interpret accurately data from models similar to the present type, mass-density-ratio effects should be thoroughly explored.

4. At 16° sweepback angle, reducing the wing aspect ratio (full span) from 9 to 8 increased the flutter speed significantly at subsonic and transonic speeds. Thus, the higher-aspect-ratio wing was more susceptible to flutter.

Horizontal-Tail Models

The results obtained with the all-movable horizontal-tail models are as follows:

1. The flutter-speed boundary rose only slightly and remained at a nearly constant level at the low supersonic Mach numbers following the transonic dip. This somewhat unusual trend indicated that for a low-altitude flight profile which extends into the supersonic region, the critical speed region flutterwise occurs at low supersonic Mach numbers.

2. A difference in the supersonic flutter data from two different wind tunnels was observed and was attributed primarily to differences in mass-density ratios obtained at flutter in the test facilities.

3. Simplified flutter-speed calculations made for the higher supersonic Mach numbers indicated that the present experimental supersonic trend was reasonable.

Vertical-Tail Models

The results obtained with the vertical-tail models are as follows:

1. The flutter-speed boundary for the models with a tip weight (radome) was typical of those for surfaces of moderate sweep and aspect ratio. The transonic Mach numbers were indicated to be the flutter critical speed region.

2. Removal of the tip weight only slightly increased the flutter dynamic pressure at near sonic speeds. The rudder rotational stiffness was indicated to be a significant parameter affecting the flutter speed of this component.

Langley Research Center,
National Aeronautics and Space Administration,
Langley Station, Hampton, Va., February 2, 1966.

REFERENCES

1. Head, A. L., Jr.: A Philosphy of Design for Flutter. Proceedings of the National Specialists Meeting on Dynamics and Aeroelasticity (Fort Worth, Texas), Inst. Aeron. Sci., Nov. 1958, pp. 59-65.

2. Mahaffey, P. T.: The Use of Low Speed Flutter Model Tests and Trend Curves To Establish Flutter Boundaries. Proceedings of the National Specialists Meeting on Dynamics and Aeroelasticity (Fort Worth, Texas), Inst. Aeron. Sci., Nov. 1958, pp. 66-68.

3. Mechtly, E. A.: The International System of Units – Physical Constants and Conversion Factors. NASA SP-7012, 1964.

4. Ruhlin, Charles L.; Sandford, Maynard C.; and Yates, E. Carson, Jr.: Wind-Tunnel Flutter Studies of the Sweptback T-Tail of a Large Multijet Cargo Airplane at Mach Numbers to 0.90. NASA TN D-2179, 1964.

5. Yates, E. Carson, Jr.; Land, Norman S.; and Foughner, Jerome T., Jr.: Measured and Calculated Subsonic and Transonic Flutter Characteristics of a 45° Sweptback Wing Planform in Air and in Freon-12 in the Langley Transonic Dynamics Tunnel. NASA TN D-1616, 1963.

6. Castile, George E.; and Herr, Robert W.: Some Effects of Density and Mach Number on the Flutter Speed of Two Uniform Wings. NACA TN 1989, 1949.

7. Barmby, J. G.; Cunningham, H. J.; and Garrick, I. E.: Study of Effects of Sweep on the Flutter of Cantilever Wings. NACA Rept. 1014, 1951. (Supersedes NACA TN 2121.)

8. Platt, Robert J., Jr.: Transonic Investigation of the Effects of Pitch Stiffness and Mass Balance on the Flutter Characteristics of an All-Movable Horizontal Tail. NASA TM X-266, 1960.

9. Morgan, Homer G.; Huckel, Vera; and Runyan, Harry L.: Procedure for Calculating Flutter at High Supersonic Speed Including Camber Deflections, and Comparison With Experimental Results. NACA TN 4335, 1958.

TABLE I.- GEOMETRIC PROPERTIES OF MODELS

Wing ($\Lambda = 16^{o}$):		
Aspect ratio of full-span wing including fuselage-sting intercept	9.2	7.9
Sweepback angle of quarter-chord line	12^{o}	12^{o}
Taper ratio of movable panel	0.29	0.37
Mean aerodynamic chord of full-span wing including fuselage-sting intercept (2b)	0.225 ft (0.0686 m)	0.232 ft (0.0707 m)
Pivot-axis location –		
Fraction of exposed semispan	0.09	0.11
Fraction of movable-panel root chord	0.26	0.26

Horizontal tail:	
Aspect ratio of exposed panel	1.06
Sweepback angle of quarter-chord line	50^{o}
Taper ratio of exposed panel	0.19
Mean aerodynamic chord of exposed panel (2b)	0.490 ft (0.149 m)
Pitch-axis sweepback angle	20^{o}
Pitch-axis location –	
Fraction of streamwise chord at exposed panel root	0.46
Fraction of streamwise mean aerodynamic chord	0.25
Vertical tail:	
Aspect ratio of exposed panel	1.16
Sweepback angle of quarter-chord line	50^{o}
Taper ratio of exposed panel	0.26
Mean aerodynamic chord of exposed panel (2b)	0.504 ft (0.154 m)
Rudder area of exposed panel, fraction of total tail area	0.30

TABLE II.- PHYSICAL PROPERTIES OF MODELS

(a) Wing models ($\Lambda = 16^{\circ}$)

Model	b		t/c	m_w		v_w	
	ft	m		slugs	kg	cu ft	m^3
Aspect-ratio-9 wing							
W1	0.113	0.0344	0.0185	0.00257	0.0375	0.0216	0.000612
W2	.113	.0344	.0249	.00353	.0515	.0216	.000612
W3	.113	.0344	.0334	.00493	.0719	.0216	.000612
W4	.113	.0344	.0392	.00575	.0839	.0216	.000612
Aspect-ratio-8 wing							
W3	0.116	0.0354	0.331	0.00477	0.0696	0.0210	0.000594
W4	.116	.0354	.391	.00560	.0817	.0210	.000594

(b) Horizontal-tail models

Model	b		t/c	m_h		v_h		I (*)	
	ft	m		slugs	kg	cu ft	m^3	slug-ft^2	kg-m^2
H1	0.245	0.0747	0.0128	0.00676	0.0986	0.0726	0.00206	2.56×10^{-4}	3.46×10^{-4}
H2	.245	.0747	.0167	.00801	.1169	.0726	.00206	2.89	3.91
H3	.245	.0747	.0191	.00937	.1367	.0726	.00206	3.21	4.35

*Includes exposed surface and torque bar; $I_{tb} = 0.10 \times 10^{-4}$ slug-ft^2 (0.135×10^{-4} kg-m^2).

(c) Horizontal-tail pitch-spring models

Spring	Thickness		K (measured values)	
	inch	cm	ft-lb/rad	m-N/rad
A	0.075	0.190	58.7	79.7
B	.080	.203	83.3	113.0
C	.090	.229	----	-----
D	.188	.478	----	-----

(d) Vertical-tail models

Model	b		t/c	m_v with tip weight (†)		m_v without tip weight		v_v	
	ft	m		slugs	kg	slugs	kg	cm ft	m^3
V1	0.252	0.0768	0.0128	0.00940	0.1372	0.00898	0.1310	0.100	0.00283
V2	.252	.0768	.0101	.01319	.1925	.01260	.1839	.100	.00283

†Center of gravity of tip weight was located at 0.77 of streamwise tip chord.

TABLE III.- MEASURED NATURAL FREQUENCIES OF MODELS

(a) Wing models

Model	f_1, cps	f_2, cps	f_3, cps	f_1/f_3	f_2/f_3
		Aspect-ratio-9 wing			
W1-1	34.7	106	205	0.169	0.517
W2-1	47.7	143	278	.172	.514
W2-2	48.2	147	282	.171	.521
W2-3	47.9	145	281	.170	.516
W2-4	48.2	147	280	.172	.525
W2-5	48.0	146	286	.168	.510
W3-1	62.5	192	372	.168	.516
W3-2	62.0	189	366	.169	.516
W4-1	74.0	239	453	.162	.528
W4-2	74.0	239	453	.162	.528
		Aspect-ratio-8 wing			
W3-3	70.5	247	401	0.176	0.616
W4-2	83.0	302	491	.169	.615

(b) Horizontal-tail models

Model	f_1, cps	f_2, cps	f_3, cps	f_2/f_1	f_3/f_1
H1A-1	63.0	161	287	2.56	4.56
H1A-2	61.5	154	316	2.50	5.14
H2A-1	69.0	178	305	2.58	4.42
H2B-1	71.9	182	340	2.53	4.73
H2C-2	79.0	192	333	2.44	4.22
H3D-1	88.0	237	453	2.69	5.15
H3C-2	74.8	203	373	2.71	4.99

(c) Vertical-tail models

Model	f_1, cps	f_2, cps	f_3, cps	f_1/f_3	f_2/f_3
		With tip weight			
V1-1	45.4	117	162	0.280	0.722
V1-2	43.5	120	157	.277	.764
V2-1	67.0	177	269	.249	.658
V2-2	66.5	175	269	.247	.651
V2-3	69.9	185	278	.251	.665
V2-4	66.8	179	261	.256	.685
V2-5	69.0	179	259	.266	.691
V2-6	69.5	176	265	.262	.664
V2-7	71.0	188	271	.262	.694
V2-8	68.0	175	262	.260	.668
V2-9	72.5	182	289	.251	.630
V2-10	70.0	183	272	.257	.673
V2-11	70.0	183	272	.257	.673
		Without tip weight			
V2-8	98.5	258	512	0.196	0.505
V2-12	91.8	286	501	.183	.571

TABLE IV.- TABULATED NONDIMENSIONAL MODE SHAPE DATA OF TYPICAL MODELS

(a) Aspect-ratio-9 wing

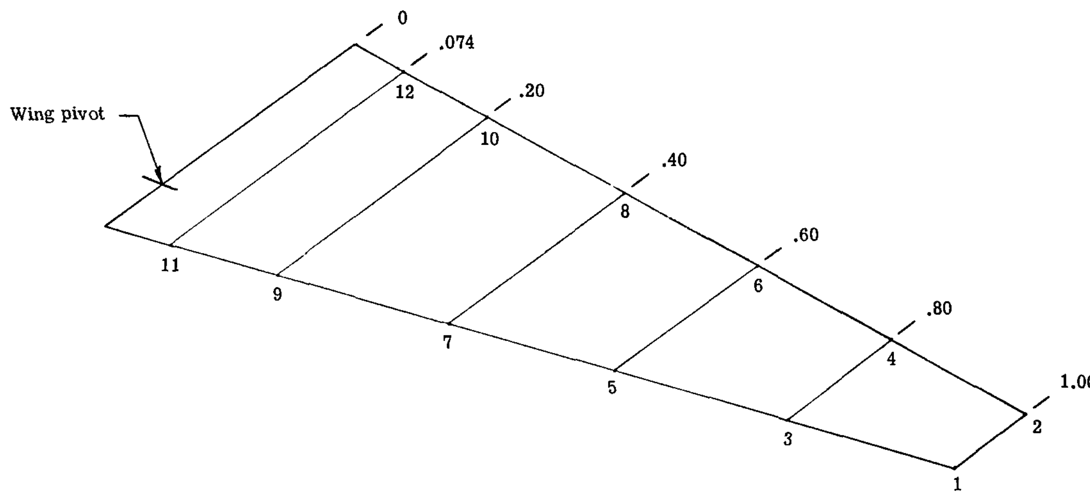

Point number	Nondimensional deflection of model W1*			Nondimensional deflection of model W2*			Nondimensional deflection of model W3*			Nondimensional deflection of model W4*		
	f_1 = 34.6 cps	f_2 = 106.1 cps	f_3 = 204.8 cps	f_1 = 47.2 cps	f_2 = 142.8 cps	f_3 = 277.9 cps	f_1 = 62.0 cps	f_2 = 190.1 cps	f_3 = 368.6 cps	f_1 = 73.6 cps	f_2 = 236.1 cps	f_3 = 454.2 cps
1	0.97	0.94	0.55	0.92	0.94	0.59	0.97	0.77	0.51	0.99	1.05	0.58
2	1.00	1.00	1.00	1.00	1.00	1.00	1.00	1.00	1.00	1.00	1.00	1.00
3	.62	.11	-.67	.63	.10	-.63	.64	.19	-.43	.48	.17	-.28
4	.64	.12	.11	.65	.12	.55	.67	.22	.07	.48	.17	.01
5	.34	-.27	-.59	.35	-.25	-.60	.36	-.29	-.43	.25	-.12	-.21
6	.40	-.28	.11	.37	-.27	.09	.37	-.30	.09	.27	-.17	.01
7	.19	-.20	-.25	.14	-.20	-.20	.14	-.25	-.17	.11	-.15	-.05
8	.18	-.27	.46	.19	-.28	.48	.18	-.33	.31	.13	-.21	.13
9	.03	-.05	-.08	.02	-.05	-.07	.03	-.07	-.05	.03	-.05	-.01
10	.07	-.15	.50	.06	-.16	.51	.06	-.18	.27	.06	-.14	.24
11	0	-.01	-.03	.01	-.01	-.02	.01	-.01	-.03	.01	-.01	-.01
12	.02	-.07	.42	.02	-.08	.44	.02	-.10	.32	.03	-.12	.27

*Out-of-phase displacement indicated by negative sign.

TABLE IV.- TABULATED NONDIMENSIONAL MODE SHAPE DATA OF TYPICAL MODELS – Continued

(b) Horizontal tail

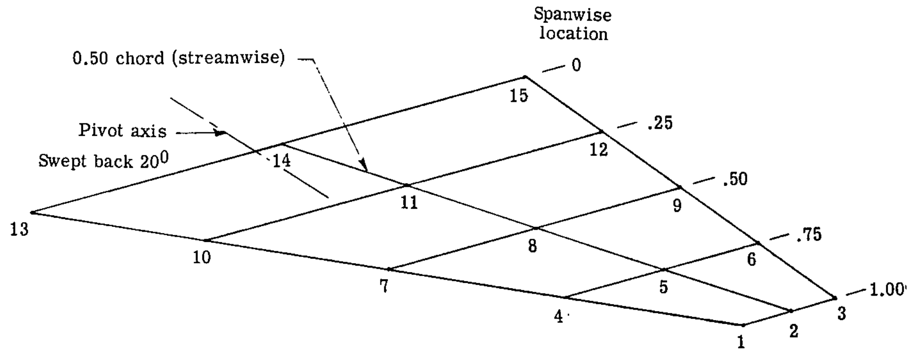

Point number	Nondimensional deflection of model H1A*			Nondimensional deflection of model H2A*			Nondimensional deflection of model H3D*			Nondimensional deflection of model H3C*		
	f_1 = 63.6 cps	f_2 = 162.1 cps	f_3 = 286.0 cps	f_1 = 68.0 cps	f_2 = 176.0 cps	f_3 = 299.4 cps	f_1 = 93.8 cps	f_2 = 247.4 cps	f_3 = 434.3 cps	f_1 = 75.7 cps	f_2 = 208.0 cps	f_3 = 405.4 cps
1	0.83	1.00	0.40	0.79	0.91	0.53	0.88	0.95	0.37	0.85	0.95	0.42
2	.89	1.00	.72	.90	.94	.77	.94	.96	.60	.90	.97	.72
3	1.00	1.00	1.00	1.00	1.00	1.00	1.00	1.00	1.00	1.00	1.00	1.00
4	.55	.60	-.17	.46	.45	-.13	.45	.52	-.45	.47	.50	-.15
5	.64	.53	-.05	.56	.37	.05	.56	.34	-.11	.55	.41	.10
6	.86	.50	.26	.84	.39	.22	.78	.35	.50	.85	.40	.28
7	.12	.34	-.22	.09	.23	-.14	.09	.28	-.31	.07	.29	-.23
8	.37	.14	-.13	.32	.11	-.09	.32	.10	-.21	.34	.15	-.14
9	.71	-.07	.05	.60	-.01	.01	.63	-.11	.09	.67	.01	.03
10	-.12	.33	-.11	-.11	.22	-.10	-.07	.22	-.08	-.14	.25	-.16
11	.15	-.02	-.10	.14	.01	-.07	.12	-.01	-.12	.15	.01	-.12
12	.56	-.41	-.02	.50	-.21	-.03	.47	-.38	.02	.52	-.26	-.06
13	-.18	.37	-.08	-.20	.28	-.09	-.14	.25	.02	-.26	.33	-.15
14	.04	-.03	-.03	.06	.01	-.03	.02	-.01	-.03	.04	-.01	-.05
15	.44	-.57	.01	.30	-.23	-.02	.36	-.46	.03	.46	-.40	-.06

*Out-of-phase displacement indicated by negative sign.

TABLE IV.- TABULATED NONDIMENSIONAL MODE SHAPE DATA OF TYPICAL MODELS – Concluded

(c) Vertical tail with tip weight

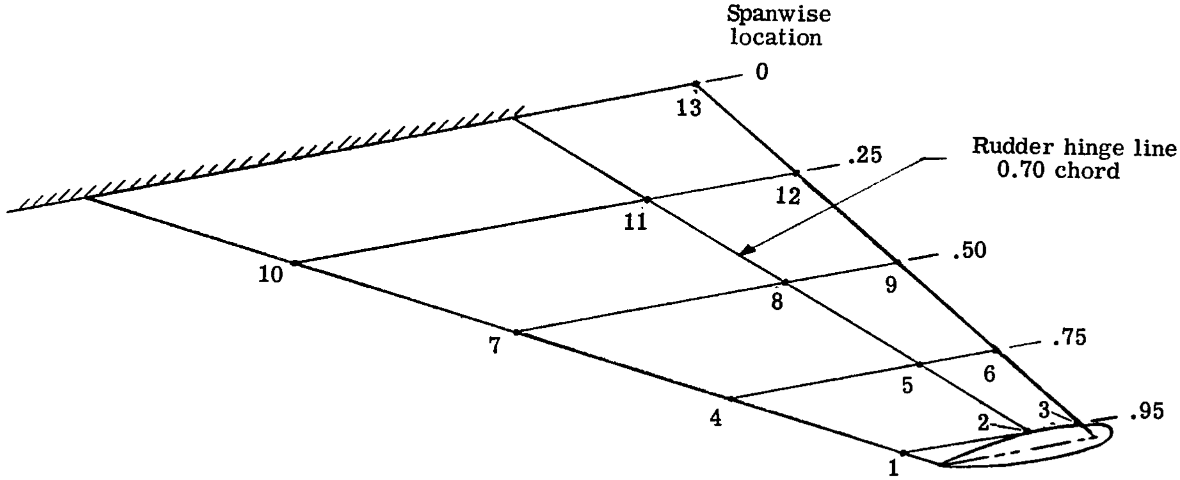

Point number	Nondimensional deflection of model V1*			Nondimensional deflection of model V2*		
	f_1 = 44.0 cps	f_2 = 112.5 cps	f_3 = 154.0 cps	f_1 = 68.6 cps	f_2 = 176.3 cps	f_3 = 269.8 cps
1	0.67	0.41	1.00	0.66	1.00	1.00
2	.85	-.10	.35	.82	-.09	.29
3	1.00	.27	-.09	1.00	.31	-.25
4	.30	.43	.82	.24	.91	.70
5	.57	.46	.67	.51	.86	.30
6	.74	.75	-.18	.60	.83	-.30
7	.06	.13	.28	.05	.27	.27
8	.28	.34	.41	.20	.70	.21
9	.43	1.00	-.40	.29	.87	-.53
10	0	.01	.02	0	.02	.02
11	.07	.13	.15	.05	.20	.03
12	.25	1.00	-.82	.14	.65	-.66
13	.10	.78	-.80	.06	.43	-.66

*Out-of-phase displacement indicated by negative sign.

TABLE V.- SUMMARY OF RESULTS

Model behavior code: F – Start of flutter
EF – End of flutter
NF – No flutter
D – Low damping

(a) Aspect-ratio-9 wing

Model	Run-point number	Model behavior	M	q		V		ρ		μ	$V/b\omega_3\sqrt{\mu}$	f, cps
				lb/sq ft	kN/m^2	ft/sec	m/s	slugs/cu ft	kg/m^3			
$\Lambda = 16^{\circ}$												
W2-3	1-1	F	0.539	480	22.9	581	177	0.00284	1.46	57.5	0.384	160
	2-1	F	.553	504	24.1	588	179	.00291	1.50	56.1	.394	184
	3-1	F	.567	492	23.5	606	185	.00267	1.38	61.2	.388	183
	4-1	F	.604	484	23.1	645	196	.00233	1.20	70.1	.386	172
W3-1	5-1	F	.786	942	45.1	821	250	.00279	1.44	81.8	.343	172
	6-1	F	.807	949	45.4	838	255	.00270	1.39	84.5	.345	171
	7-1	F	.941	975	46.6	964	294	.00209	1.08	109.2	.349	150
	8-1	F	.624	1169	55.9	641	195	.00568	2.93	40.1	.382	211
	9-1	F	.850	854	40.8	867	264	.00227	1.17	100.5	.327	161
	-2	EF	.948	1004	48.0	952	290	.00221	1.14	103.2	.354	150
	-3	F	.947	984	47.1	941	287	.00222	1.14	102.8	.351	139
	-4	EF	.830	815	39.0	839	256	.00232	1.20	98.3	.320	158
	10-1	F	.928	1011	48.4	892	272	.00254	1.31	89.8	.356	138
	-2	EF	.808	829	39.6	791	241	.00265	1.36	86.1	.322	156
	11-1	F	1.186	2971	142.2	1074	327	.00515	2.65	44.3	.610	350
	12-1	F	.671	1068	51.1	696	212	.00441	2.27	51.7	.366	200
	13-1	F	1.249	3777	180.8	1163	354	.00558	2.88	40.9	.688	350
	-2	*EF	1.132	2771	132.6	997	304	.00457	2.36	49.9	.534	---
	14-1	F	.933	1526	73.0	918	280	.00362	1.86	63.0	.437	200
W3-2	15-1	F	.588	1319	63.1	606	185	.00716	3.69	31.8	.413	230
	16-1	F	.571	1261	60.3	583	178	.00742	3.82	30.7	.404	230
	17-1	F	1.068	1954	93.5	1010	308	.00382	1.97	59.7	.502	350
	-2	EF	.960	1803	86.3	922	281	.00424	2.18	53.8	.483	320
	-3	F	.939	1776	85.0	905	276	.00433	2.23	52.7	.479	207
	18-1	F	1.058	1675	75.4	1008	307	.00329	1.70	69.3	.465	350
	-2	EF	1.005	1590	76.1	964	294	.00342	1.76	66.7	.454	360
	-3	F	.945	1431	68.5	914	278	.00342	1.76	66.7	.430	177
	19-1	F	1.065	1413	67.6	1024	312	.00269	1.39	84.8	.427	367
	-2	EF	1.052	1410	67.5	1014	309	.00274	1.41	83.3	.427	350
	-3	F	.942	1286	61.5	923	281	.00301	1.55	75.8	.407	183
	20-1	F	.854	862	41.2	874	266	.00226	1.16	100.9	.334	165
	-2	EF	.945	995	47.6	951	290	.00220	1.13	103.7	.359	133
	-3	F	1.069	1153	55.2	1052	321	.00208	1.07	109.7	.386	375
	-4	EF	1.084	1185	56.7	1063	324	.00210	1.08	108.6	.392	350
	-5	*F	.951	982	47.0	946	288	.00219	1.13	104.2	.356	133
	-6	*EF	.835	825	39.5	845	258	.00231	1.19	98.8	.327	160
W4-1	21-1	F	.869	1431	68.5	894	272	.00358	1.84	74.3	.322	167
	22-1	F	.793	2153	103.0	811	247	.00653	3.36	40.7	.394	220
	23-1	F	.862	1401	67.0	894	272	.00350	1.80	76.0	.318	167
	24-1	F	.839	1764	84.4	864	263	.00472	2.43	56.4	.357	183
	25-1	F	.901	1365	65.3	932	284	.00314	1.62	84.7	.314	148
	-2	EF	.928	1508	72.2	956	291	.00330	1.70	80.6	.330	148
	26-1	F	.908	1938	92.7	904	276	.00473	2.44	56.2	.374	167
	27-1	F	.915	2470	118.2	900	274	.00609	3.14	43.7	.423	200
	-2	EF	.807	1953	93.5	801	244	.00607	3.13	43.8	.376	218
	28-1	D	.727	2311	110.6	734	224	.00856	4.41	31.1	.409	250
	-2	F	.729	2529	121.0	721	220	.00971	5.00	27.4	.428	239
	29-1	F	.818	1992	95.3	886	270	.00506	2.61	52.6	.379	208
	30-1	NF	1.251	4370	209.2	1149	350	.00662	3.41	40.2	.563	---
	31-1	F	.917	1328	63.5	950	290	.00294	1.52	90.5	.310	150
	-2	EF	.932	1404	67.2	964	294	.00302	1.56	88.1	.319	140
	-3	NF	1.069	3836	183.6	1019	310	.00738	3.80	36.0	.527	---
	-4	*F	.925	2733	130.8	887	270	.00693	3.57	38.4	.444	220
W4-2	32-1	F	.705	2184	104.5	735	224	.00809	4.17	32.9	.398	236

*Data point obtained during tunnel shutdown conditions.

Model	Run-point number	Model behavior	M	q		V		ρ		μ	$V/b\omega_3\sqrt{\mu}$	f, cps
				lb/sq ft	kN/m^2	ft/sec	m/s	slugs/cu ft	kg/m^3			
$\Lambda = 39^{\circ}$												
W3-2	33-1	F	0.863	871	41.7	893	272	0.00218	1.12	104.7	0.335	158
	34-1	F	.574	1436	68.7	601	183	.00794	4.09	28.7	.431	275
	35-1	F	.888	907	43.4	910	277	.00219	1.13	104.2	.343	160
W3-1	36-1	F	.691	1297	62.1	713	217	.00510	2.63	44.7	.403	274
	37-1	F	.765	1315	62.9	790	241	.00421	2.17	54.2	.406	265
	38-1	F	.828	1234	59.0	848	258	.00343	1.77	66.5	.393	188
	39-1	F	.802	1251	59.9	824	251	.00368	1.90	62.0	.396	267
	40-1	F	.851	1129	54.0	872	266	.00297	1.53	76.8	.376	180
	41-1	F	.905	945	45.2	940	286	.00213	1.10	107.1	.343	150
	-2	EF	1.125	1299	62.2	1124	342	.00205	1.06	111.3	.403	150
	-3	NF	1.258	4164	199.3	1150	350	.00629	3.24	36.2	.722	---
	-4	*F	1.154	3326	159.2	1062	324	.00589	3.04	38.7	.645	300
	42-1	F	.869	1081	51.7	899	274	.00267	1.38	85.4	.368	165
	-2	EF	1.092	1777	85.0	1077	328	.00306	1.58	74.5	.472	200
	-3	F	1.150	2661	127.4	1109	338	.00432	2.23	52.8	.577	230
	43-1	F	.919	972	46.5	954	291	.00213	1.10	107.1	.348	145
	-2	EF	1.116	1266	60.6	1115	340	.00203	1.05	112.4	.398	167
	-3	F	1.136	2209	105.7	1066	325	.00388	2.00	58.8	.526	220
	44-1	F	.882	940	45.0	923	281	.00220	1.13	103.7	.343	157
	-2	EF	1.178	1424	68.1	1176	358	.00206	1.06	110.8	.423	170
	-3	F	1.166	3207	153.5	1062	324	.00568	2.93	40.1	.634	275
	-4	*EF	.801	1230	58.8	737	225	.00452	2.33	50.5	.392	225
W4-1	45-1	F	.804	2912	139.4	811	247	.00885	4.56	30.0	.459	320
	46-1	D	.897	2684	128.5	911	278	.00645	3.32	41.2	.440	270
	-2	F	.891	3164	151.4	891	272	.00796	4.10	33.4	.479	300
	47-1	D	.945	2392	114.5	974	297	.00504	2.60	52.8	.416	210
	-2	F	.950	2707	129.6	968	295	.00577	2.97	46.1	.443	227
	48-1	D	.959	2223	106.4	998	304	.00446	2.30	59.6	.401	222
	-2	F	.962	2612	125.0	995	303	.00527	2.72	50.5	.435	230
	49-1	D	.924	1584	75.8	967	295	.00338	1.74	78.7	.338	162
	-2	F	.971	2153	103.0	1003	306	.00427	2.20	62.3	.395	208
	50-1	D	.974	1751	83.8	1008	307	.00344	1.77	77.3	.356	185
	-2	F	1.004	2026	97.0	1032	314	.00380	1.96	70.0	.383	191
	51-1	D	.990	1610	77.0	1024	312	.00307	1.58	86.7	.341	171
	-2	F	1.054	2094	100.2	1073	327	.00363	1.87	73.3	.389	189
	52-1	D	.992	1436	68.7	1025	312	.00273	1.41	97.5	.322	170
	-2	F	1.057	1663	79.6	1082	330	.00284	1.46	93.7	.347	170
	-3	EF	1.094	1862	89.1	1110	338	.00302	1.56	88.1	.367	178
	-4	F	1.154	3462	165.7	1134	346	.00538	2.77	49.4	.501	238
	53-1	NF	1.257	4690	224.5	1190	363	.00662	3.41	40.2	.583	---
	54-1	D	1.182	2366	113.2	1087	331	.00400	2.06	66.5	.414	190
	-2	F	1.065	2203	105.4	991	302	.00449	2.31	59.2	.400	188
	55-1	F	1.081	1215	58.1	1098	335	.00201	1.04	132.4	.296	150
	-2	EF	1.110	1257	60.1	1122	342	.00200	1.03	133.1	.302	150
	-3	D	1.184	2951	141.2	1114	340	.00474	2.44	56.1	.462	220
	-4	F	1.092	2811	134.5	1040	317	.00519	2.67	51.2	.451	210
	-5	EF	.952	2529	121.0	922	281	.00594	3.06	44.8	.428	230
W2-5	†56-1	F	2.0	2501	119.7	1662	506	.00181	.93	90.2	.861	267
W2-4	†57-1	F	2.5	3568	170.8	1838	500	.00211	1.09	77.4	1.050	271
W3-2	†58-1	NF	2.0	4935	236.2	1635	498	.00369	1.90	61.8	.800	---

†Designates run made in VST; all undesignated runs made in TBT.

TABLE V.- SUMMARY OF RESULTS – Continued

(a) Aspect-ratio-9 wing – Concluded

Model	Run-point number	Model behavior	M	q, lb/sq ft	q, kN/m^2	V, ft/sec	V, m/s	ρ, slugs/cu ft	ρ, kg/m^3	μ	$V/b\omega_3\sqrt{\mu}$	f, cps
$\Lambda = 73^\circ$												
W2-1	59-1	D	0.786	1148	54.9	817	249	0.00343	1.77	47.6	0.599	250
	-2	F	.821	1462	70.0	844	257	.00410	2.11	39.8	.677	250
	60-1	D	.701	1208	57.8	729	222	.00454	2.34	36.0	.615	250
	-2	F	.709	1382	66.1	733	223	.00514	2.65	31.7	.658	250
	61-1	D	.839	1133	54.2	861	262	.00306	1.58	53.4	.596	255
	-2	F	.915	1518	72.6	920	280	.00358	1.84	45.6	.689	242
	62-1	D	.883	1225	58.6	900	274	.00302	1.56	54.1	.619	250
	-2	F	.894	1295	62.0	907	276	.00314	1.62	52.0	.636	255
	63-1	D	.888	1162	55.6	907	276	.00282	1.45	57.9	.603	254
	-2	F	.997	1495	71.5	995	303	.00301	1.55	54.2	.684	250
	64-1	D	1.102	1215	58.1	1092	333	.00204	1.05	80.1	.618	250
	-2	F	1.235	1704	81.5	1183	360	.00243	1.25	67.2	.730	235
	65-1	D	.640	1266	60.6	669	204	.00566	2.92	28.8	.630	244
	-2	F	.651	1650	79.0	666	203	.00743	3.83	22.0	.719	250
	66-1	D	1.071	1172	56.1	1065	325	.00206	1.06	79.3	.605	250
	-2	F	1.261	1670	79.9	1213	370	.00227	1.17	71.9	.724	250
	67-1	D	.981	1084	51.9	990	302	.00221	1.13	73.9	.583	267
	-2	F	1.227	1755	84.0	1174	358	.00254	1.31	64.3	.741	250
W3-1	68-1	D	1.089	3400	162.7	1040	317	.00628	3.24	36.3	.653	340
	-2	F	1.090	3645	174.5	1032	314	.00684	3.52	33.3	.676	340
	69-1	D	1.205	3358	160.7	1120	341	.00534	2.75	42.7	.648	330
	-2	F	1.202	3732	178.6	1101	336	.00615	3.17	37.1	.684	334
	70-1	D	1.196	3224	154.3	1116	340	.00517	2.66	44.1	.635	333
	-2	F	1.197	3881	185.8	1065	325	.00683	3.52	33.4	.697	340
	71-1	D	1.209	3293	157.6	1160	354	.00489	2.52	46.6	.642	325
	-2	F	1.207	4406	210.9	1128	344	.00692	3.57	32.9	.743	340
	72-1	D	.882	3234	154.8	884	269	.00825	4.25	27.6	.636	335
	-2	F	.880	3551	170.0	864	263	.00950	4.90	24.0	.667	342
W1-1	†73-1	F	3.0	1354	64.8	2062	628	.000636	.33	187.0	1.035	202
W2-1	†74-1	D	2.0	2635	126.1	1663	507	.00190	.98	86.0	.908	300
	-2	F	2.0	2772	132.7	1659	506	.00201	1.04	81.3	.932	300
W2-2	†75-1	F	2.5	3254	155.8	1844	562	.00191	.98	85.5	.996	280
W2-5	†76-1	NF	3.0	2953	141.3	1982	604	.00150	.77	108.9	.935	---

†Designates run made in VST; all undesignated runs made in TBT.

(b) Aspect-ratio-8 wing

Model	Run-point number	Model behavior	M	q, lb/sq ft	q, kN/m^2	V, ft/sec	V, m/s	ρ, slugs/cu ft	ρ, kg/m^3	μ	$V/b\omega_3\sqrt{\mu}$	f, cps
$\Lambda = 16^\circ$												
W3-3	77-1	F	0.896	920	44.0	924	282	0.00215	1.11	105.6	0.307	135
	78-1	D	.805	1201	57.5	841	256	.00339	1.75	67.0	.351	175
	-2	F	.825	1320	63.2	857	261	.00359	1.85	63.2	.368	175
	79-1	D	.693	1388	66.4	733	223	.00517	2.66	43.9	.378	220
	-2	F	.700	1500	71.8	738	225	.00550	2.83	41.3	.393	223
	80-1	NF	.912	1502	71.9	928	283	.00348	1.79	76.6	.296	---
W4-2	81-1	NF	.783	2698	129.1	758	231	.00938	4.83	28.4	.397	---
	82-1	F	.859	2209	105.7	874	266	.00577	2.97	46.2	.359	167
	83-1	D	.895	2046	97.9	910	277	.00494	2.54	53.9	.346	157
	-2	F	.904	2259	108.1	911	278	.00543	2.80	49.1	.363	160
	-3	EF	.910	2341	112.0	916	279	.00558	2.88	47.7	.370	162
	-4	F	.910	2887	138.2	899	274	.00714	3.68	37.3	.411	205
	-5	*EF	.823	2461	117.8	819	250	.00733	3.78	36.3	.379	191
	84-1	F	.894	2144	102.6	910	277	.00518	2.67	51.4	.354	164
	-2	EF	.876	2115	101.2	893	272	.00530	2.73	50.3	.352	167
	85-1	F	.923	3439	164.6	923	281	.00807	4.16	33.0	.449	221

*Data point obtained during tunnel shutdown conditions.

TABLE V.- SUMMARY OF RESULTS – Concluded

(c) Horizontal tail

Model	Run-point number	Model behavior	M	q, lb/sq ft	q, kN/m^2	V, ft/sec	V, m/s	ρ, slugs/cu ft	ρ, kg/m^3	μ	$V/b\omega_1\sqrt{\mu}$	f, cps
H1A-1	86-1	D	0.678	956	45.7	687	209	0.00404	2.08	23.0	1.47	133
	-2	F	.685	1067	51.0	694	212	.00443	2.28	21.0	1.56	140
	87-1	D	.595	1056	50.5	626	191	.00537	2.77	17.3	1.55	133
	-2	F	.612	1233	59.0	641	195	.00599	3.09	15.5	1.67	133
	88-1	D	.744	927	44.3	775	236	.00309	1.59	30.1	1.45	133
	-2	F	.763	1002	47.9	790	241	.00321	1.65	29.0	1.51	133
	89-1	D	.783	899	43.0	809	246	.00274	1.41	33.9	1.43	138
	-2	F	.827	1009	48.3	847	258	.00281	1.45	33.1	1.51	133
H2A-1	90-1	D	.795	1859	89.0	815	248	.00559	2.88	19.7	1.72	150
	-2	F	.803	2396	114.7	805	245	.00739	3.81	14.9	1.96	158
	91-1	D	.863	2019	96.6	878	268	.00523	2.70	21.1	1.80	157
	-2	F	.869	2389	114.3	875	267	.00624	3.22	17.6	1.95	160
	92-1	F	.898	1873	89.6	905	276	.00457	2.36	24.1	1.73	150
	93-1	F	.905	1626	77.8	914	278	.00389	2.00	28.3	1.61	156
	94-1	F	.932	1498	71.7	933	284	.00344	1.77	32.0	1.55	150
	95-1	F	.951	1375	65.8	950	290	.00305	1.57	36.1	1.48	133
	-2	EF	.963	1420	67.9	959	292	.00308	1.59	35.8	1.50	133
	96-1	D	1.203	1473	70.5	1156	352	.00220	1.13	50.1	1.53	140
	-2	F	1.233	1768	84.6	1172	357	.00257	1.32	42.9	1.68	150
	97-1	F	.951	1292	61.8	932	284	.00297	1.53	37.1	1.44	132
	-2	EF	.933	1259	60.2	917	280	.00299	1.54	36.9	1.42	---
	98-1	D	1.228	1801	86.2	1162	354	.00267	1.38	41.3	1.70	147
	-2	F	.932	1509	72.2	911	278	.00363	1.87	30.3	1.55	144
	-3	EF	.908	1416	67.8	888	271	.00359	1.85	30.7	1.50	144
	99-1	D	1.216	1702	81.4	1159	353	.00253	1.30	43.6	1.65	142
	-2	F	.958	1555	74.4	940	286	.00352	1.81	31.3	1.58	133
	100-1	D	1.151	1616	77.3	1116	340	.00259	1.33	42.6	1.61	150
	-2	F	1.189	1752	83.8	1143	348	.00268	1.38	41.1	1.67	150
	101-1	F	.952	1280	61.2	960	293	.00277	1.43	39.8	1.43	129
	-2	EF	.972	1345	64.4	975	297	.00282	1.45	39.1	1.46	129
	-3	D	1.053	1610	77.0	1036	316	.00299	1.54	36.9	1.60	146
	-4	F	1.102	1799	86.1	1070	326	.00313	1.61	35.2	1.69	150
	102-1	D	1.239	1918	91.8	1177	359	.00276	1.42	39.9	1.75	150
	-2	F	1.241	1806	86.4	1182	360	.00258	1.33	42.7	1.70	148
	103-1	NF	.667	2467	118.1	662	202	.01122	5.78	9.8	1.98	---
	104-1	NF	.733	2866	137.2	735	224	.01059	5.46	10.4	2.14	---
H3D-1	105-1	NF	.886	1922	92.0	880	268	.00496	2.56	26.0	1.27	---
	106-1	D	.928	2644	126.5	915	279	.00631	3.25	20.4	1.49	212
	-2	F	.929	2989	143.1	891	272	.00752	3.88	17.1	1.58	206
	107-1	NF	.944	2010	96.2	935	285	.00460	2.37	28.0	1.30	---
	108-1	F	.980	2566	122.8	971	296	.00544	2.80	23.7	1.47	190
	109-1	D	1.031	2516	120.4	1006	307	.00497	2.56	25.9	1.45	190
	-2	F	1.040	2716	130.0	1007	307	.00535	2.76	24.1	1.51	195
H3C-2	110-1	NF	.709	1820	87.1	722	220	.00698	3.60	18.4	1.45	---
	111-1	D	.724	2532	121.2	719	219	.00978	5.04	13.2	1.71	180
	-2	F	.724	2593	124.1	710	216	.01027	5.29	12.5	1.73	180
	112-1	D	.867	2125	101.7	870	265	.00561	2.89	23.0	1.57	167
	-2	F	.877	2317	110.9	875	267	.00604	3.11	21.3	1.64	167

(c) Horizontal tail – Concluded

Model	Run-point number	Model behavior	M	q, lb/sq ft	q, kN/m^2	V, ft/sec	V, m/s	ρ, slugs/cu ft	ρ, kg/m^3	μ	$V/b\omega_1\sqrt{\mu}$	f, cps
H3C-2	113-1	F	0.944	1863	89.2	947	289	0.00415	2.14	31.1	1.47	140
	114-1	D	1.020	2104	100.7	997	304	.00422	2.17	30.5	1.56	161
	-2	F	1.023	2210	105.8	997	304	.00444	2.29	29.0	1.60	165
	115-1	D	1.024	1930	92.4	1005	306	.00381	1.96	33.8	1.49	168
	-2	F	1.040	2105	100.7	1012	308	.00410	2.11	31.4	1.56	167
	116-1	D	1.194	1932	92.5	1145	349	.00294	1.52	43.9	1.50	156
	-2	F	1.197	2136	102.2	1142	348	.00327	1.68	39.4	1.57	155
	117-1	D	1.242	1941	92.9	1184	361	.00276	1.42	46.7	1.50	153
	-2	F	1.245	2192	104.9	1181	360	.00314	1.62	41.1	1.60	154
H2A-1	†118-1	D	2.0	1649	78.9	1746	532	.00108	.557	102.1	1.62	119
	-2	F	2.0	2058	98.5	1738	530	.00136	.701	81.1	1.81	125
H1A-2	‡119-1	F	2.16	1106	52.9	1881	573	.000625	3.22	148.9	1.62	105
H2B-1	‡120-1	F	1.6	1155	55.3	1575	480	.000930	.479	118.6	1.30	120
	‡121-1	NF	1.6	851	40.7	1575	480	.000686	.354	160.8	1.21	---
H2C-2	†122-1	F	2.0	2420	115.8	1711	522	.00165	.850	66.6	1.64	154
H2A-3	†123-1	F	2.5	2879	137.8	1880	573	.00162	.835	67.9	2.12	116

†Designates run made in VST; all undesignated runs made in TBT.
‡Designates run made in UPWT; all undesignated runs made in TBT.

(d) Vertical tail

Model	Run-point number	Model behavior	M	q, lb/sq ft	q, kN/m^2	V, ft/sec	V, m/s	ρ, slugs/cu ft	ρ, kg/m^3	μ	$V/b\omega_r\sqrt{\mu}$	f, cps
With tip weight												
V2-1	124-1	NF	0.859	1853	88.7	855	261	0.00506	2.61	26.0	0.393	---
	125-1	F	.866	2059	98.5	871	265	.00542	2.79	24.3	.414	180
V2-5	126-1	F	.931	1894	90.6	920	280	.00447	2.30	29.5	.413	125
V2-3	127-1	F	.957	1620	77.5	955	291	.00354	1.82	37.2	.355	112
V2-4	128-1	F	1.050	1788	85.6	1032	314	.00336	1.73	39.2	.398	117
V2-6	129-1	NF	1.244	1895	90.7	1187	362	.00269	1.39	49.0	.404	---
	130-1	F	1.241	2242	107.3	1172	357	.00326	1.68	40.4	.439	200
V2-7	131-1	F	.899	2051	98.2	902	275	.00503	2.59	26.2	.410	125
V2-10	132-1	NF	.945	1524	72.9	955	291	.00334	1.72	39.4	.352	---
	133-1	NF	.785	2059	98.5	788	240	.00662	3.41	19.9	.410	---
	134-1	F	.801	1984	94.9	847	258	.00552	2.84	23.8	.402	125
V2-8	135-1	D	1.255	1846	88.3	1227	374	.00245	1.26	53.8	.403	120
	-2	F	1.248	1899	90.9	1218	371	.00255	1.31	51.7	.408	121
V2-9	136-1	D	1.060	1712	81.9	1064	324	.00302	1.56	43.6	.351	120
	-2	F	1.103	1961	93.9	1097	334	.00325	1.67	40.5	.376	125
V2-11	137-1	F	.686	1853	88.7	711	217	.00732	3.77	18.0	.388	128
V1-2	‡138-1	F	1.600	1048	50.1	1575	480	.000844	.435	111.3	.600	91
V1-1	‡139-1	F	2.160	1672	80.0	1881	573	.000946	.488	99.3	.735	100
Without tip weight												
V2-8	140-1	D	1.237	1591	76.1	1209	368	0.00218	1.12	57.8	0.389	280
	-2	F	1.252	2311	110.6	1211	369	.00314	1.62	40.1	.467	275
V2-12	141-1	F	1.019	2169	103.8	1015	309	.00421	2.17	29.9	.410	188

‡Designates run made in UPWT; all undesignated runs made in TBT.

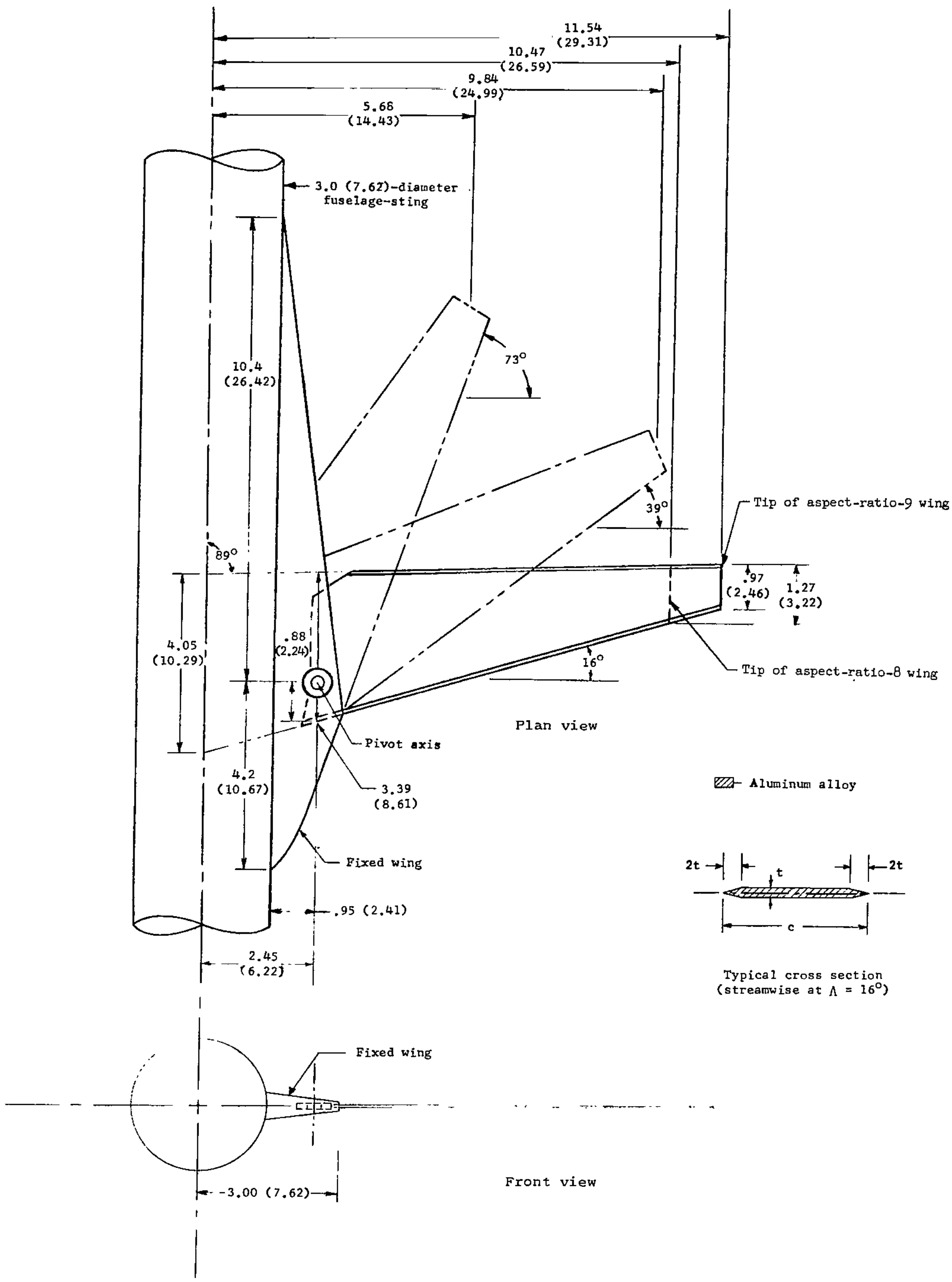

(a) Wings.

Figure 1.- Sketches of models mounted on fuselage-sting used in Langley 26-inch transonic blowdown tunnel. All linear dimensions are in inches (centimeters).

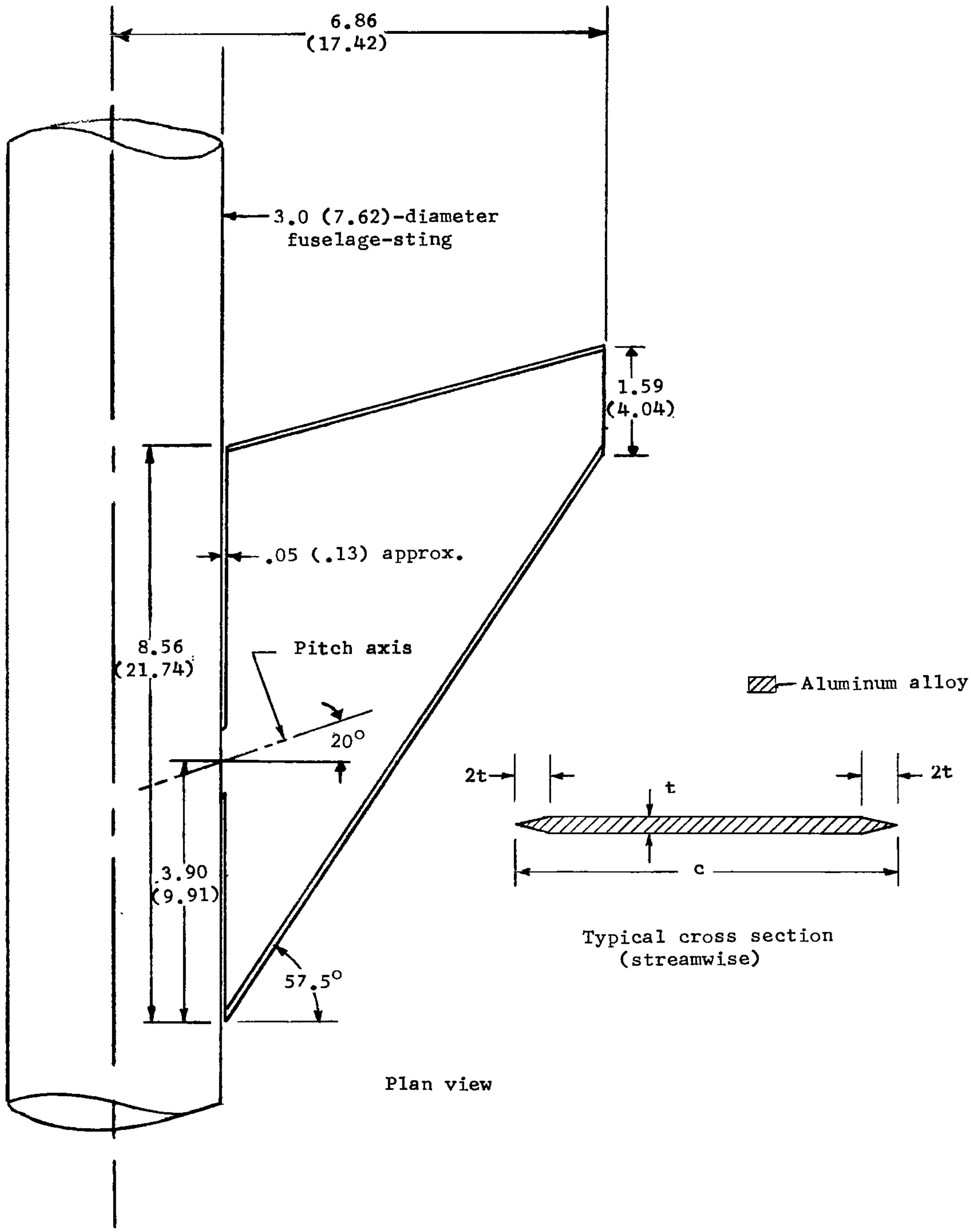

(b) Horizontal tail.

Figure 1.- Continued.

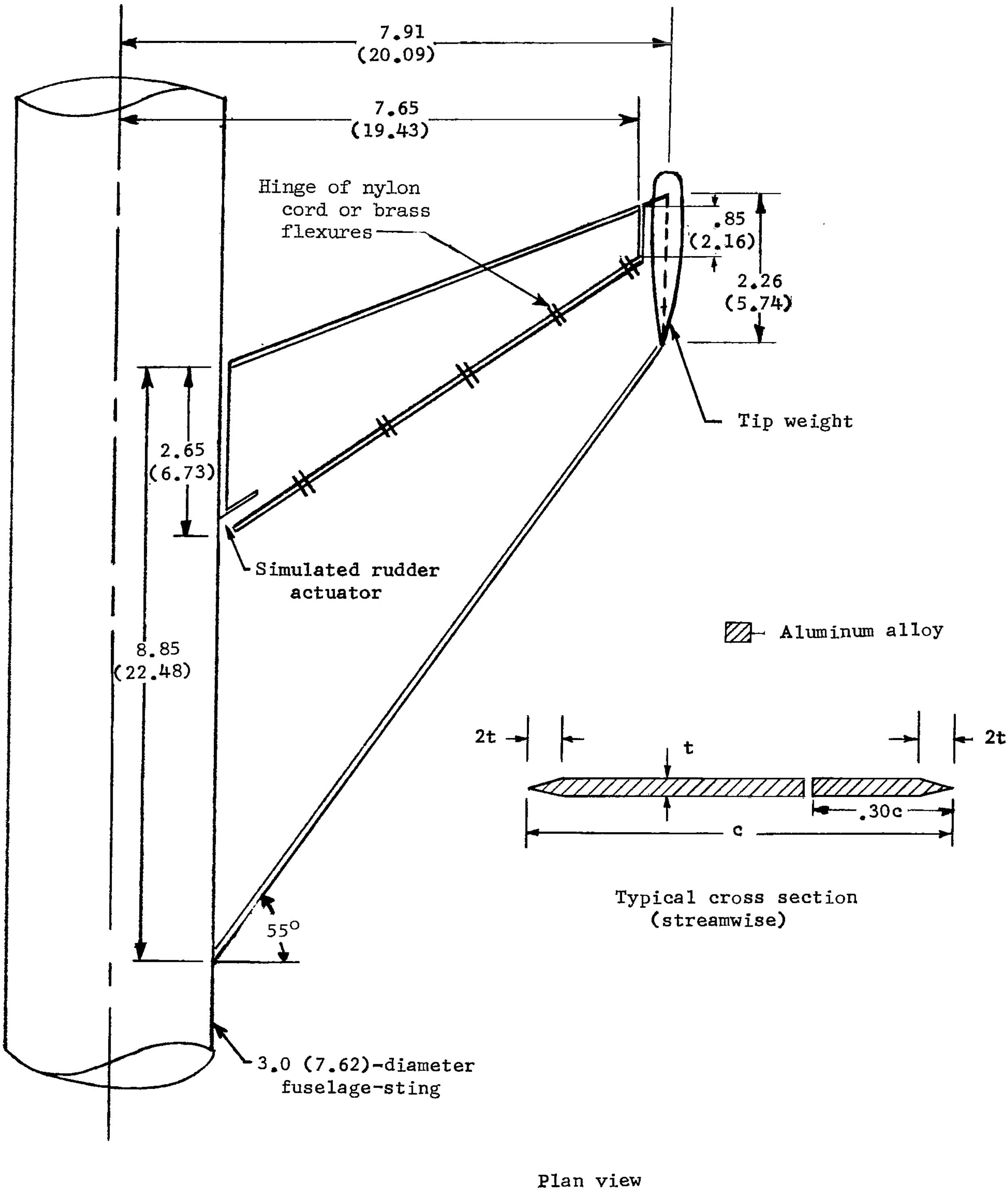

(c) Vertical tail.

Figure 1.- Concluded.

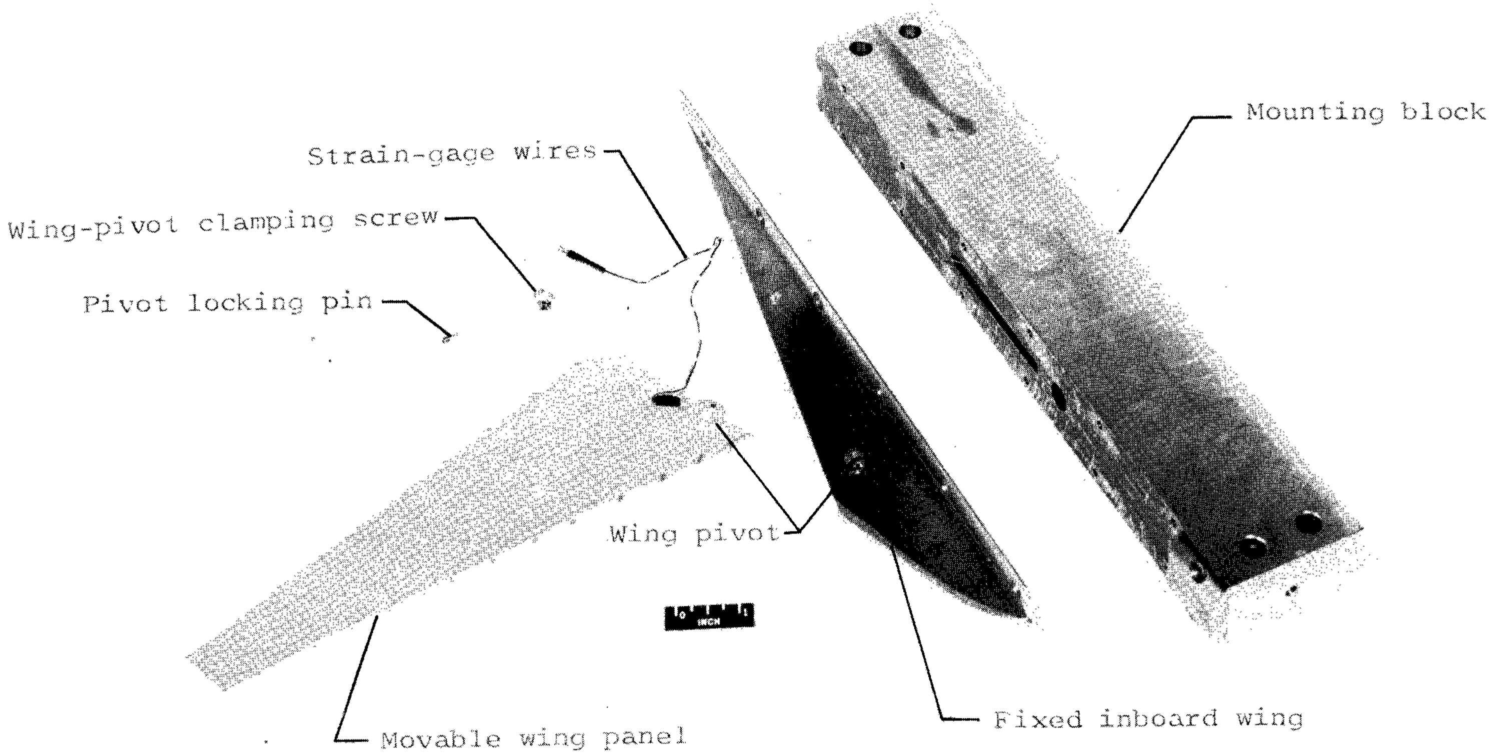

(a) Aspect-ratio-9 wing model. L-63-607.1

Figure 2.- Photographs of models.

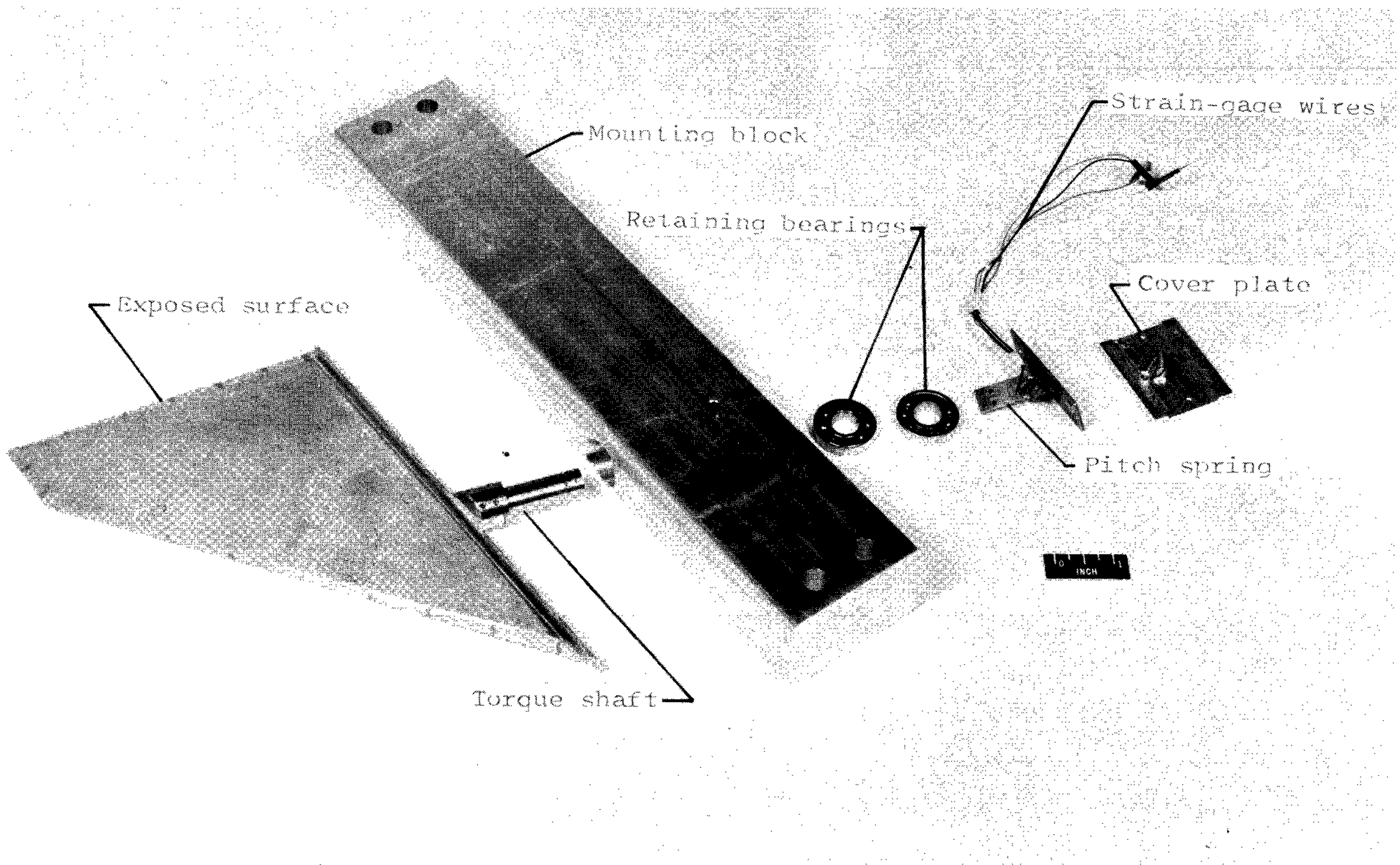

(b) Horizontal-tail model. L-63-602.1

Figure 2.- Continued.

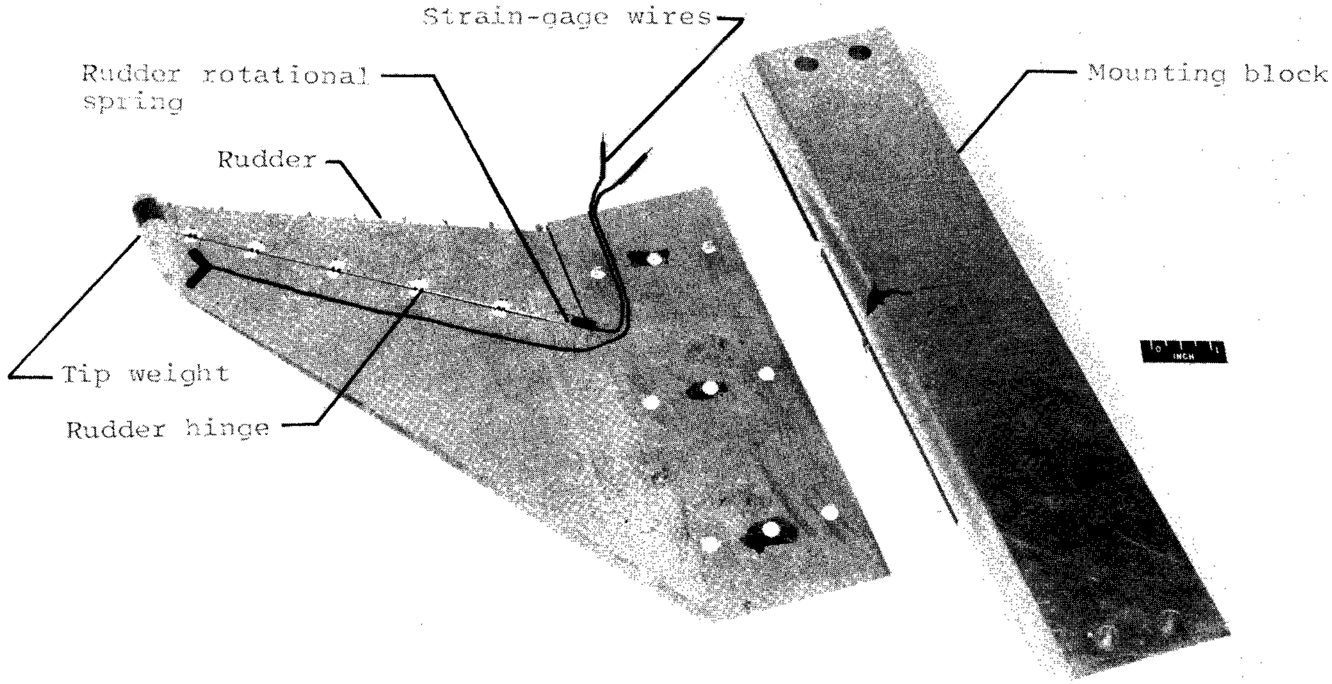

(c) Vertical-tail model.

L-63-603.1

Figure 2.- Concluded.

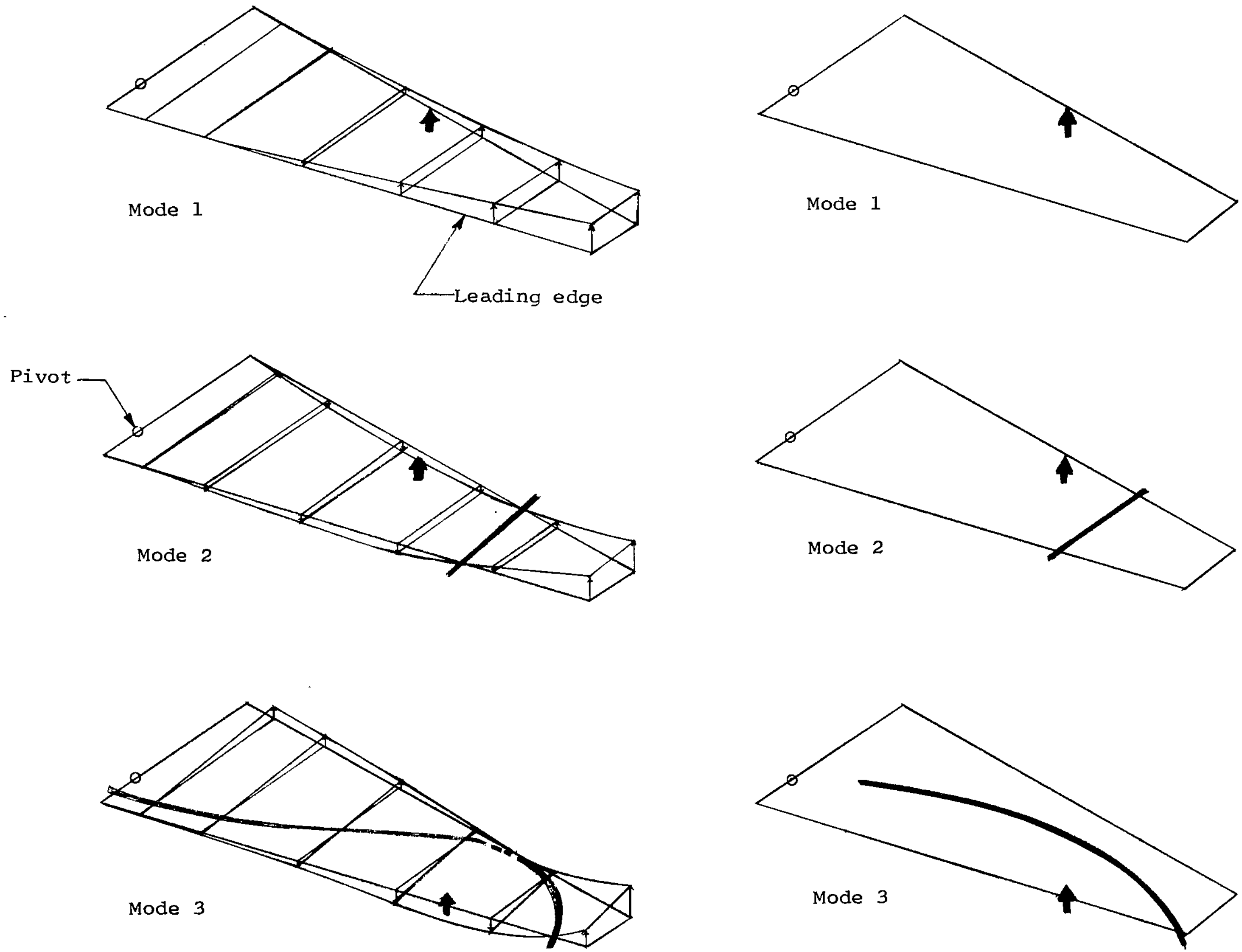

Typical aspect-ratio-9 wing model

Typical aspect-ratio-8 wing model

(a) Wings.

Figure 3.- Measured mode shapes and node lines of models. Heavy arrow indicates shaker location.

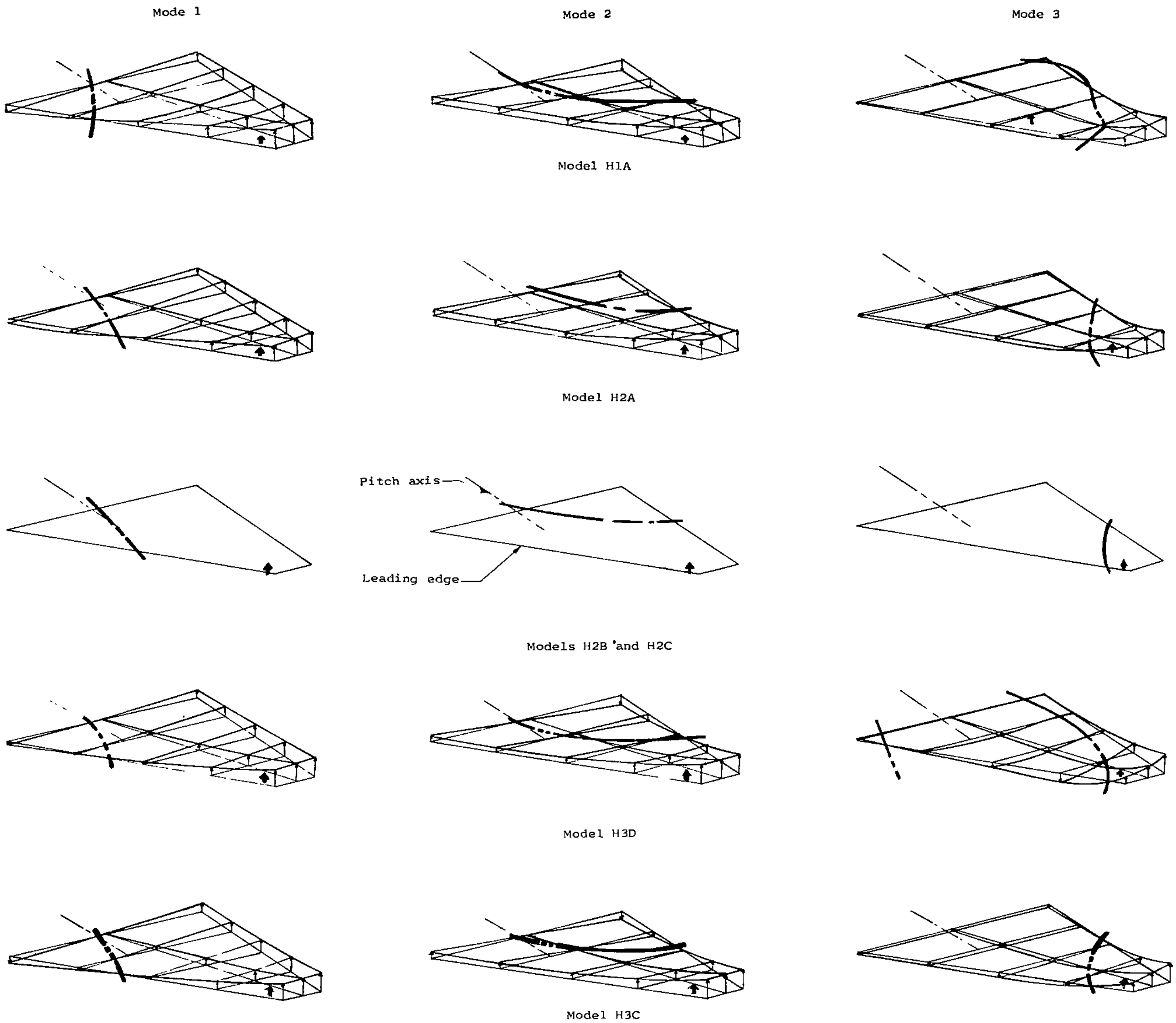

(b) Horizontal tails.

Figure 3.- Continued.

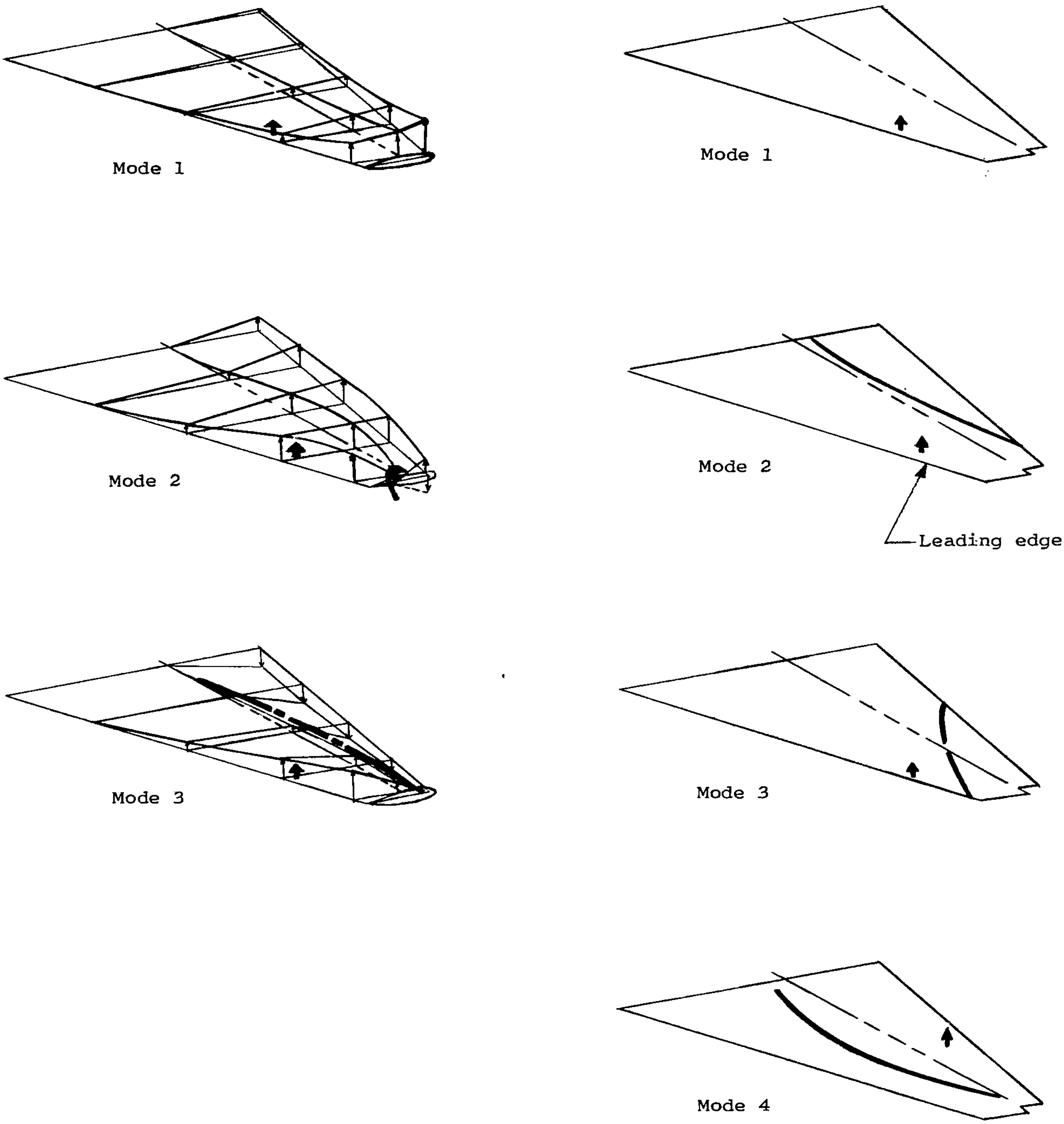

Typical model with tip weight

Typical model without tip weight

(c) Vertical tails.

Figure 3.- Concluded.

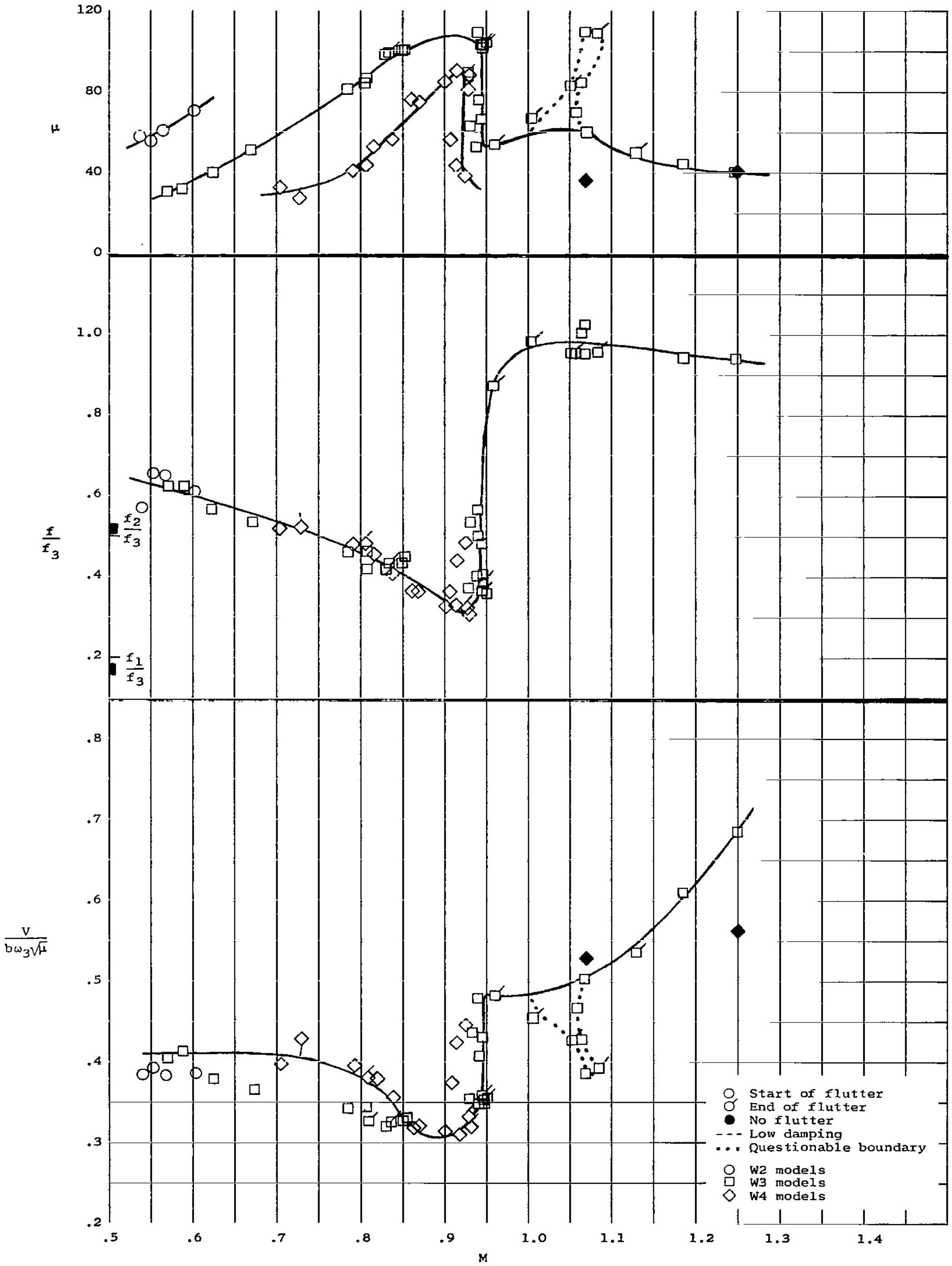

(a) Aspect-ratio-9 wing at $\Lambda = 16^0$.

Figure 4.- Variation of flutter-speed index, flutter-frequency ratio, and mass-density ratio with Mach number for wings at various sweepback angles.

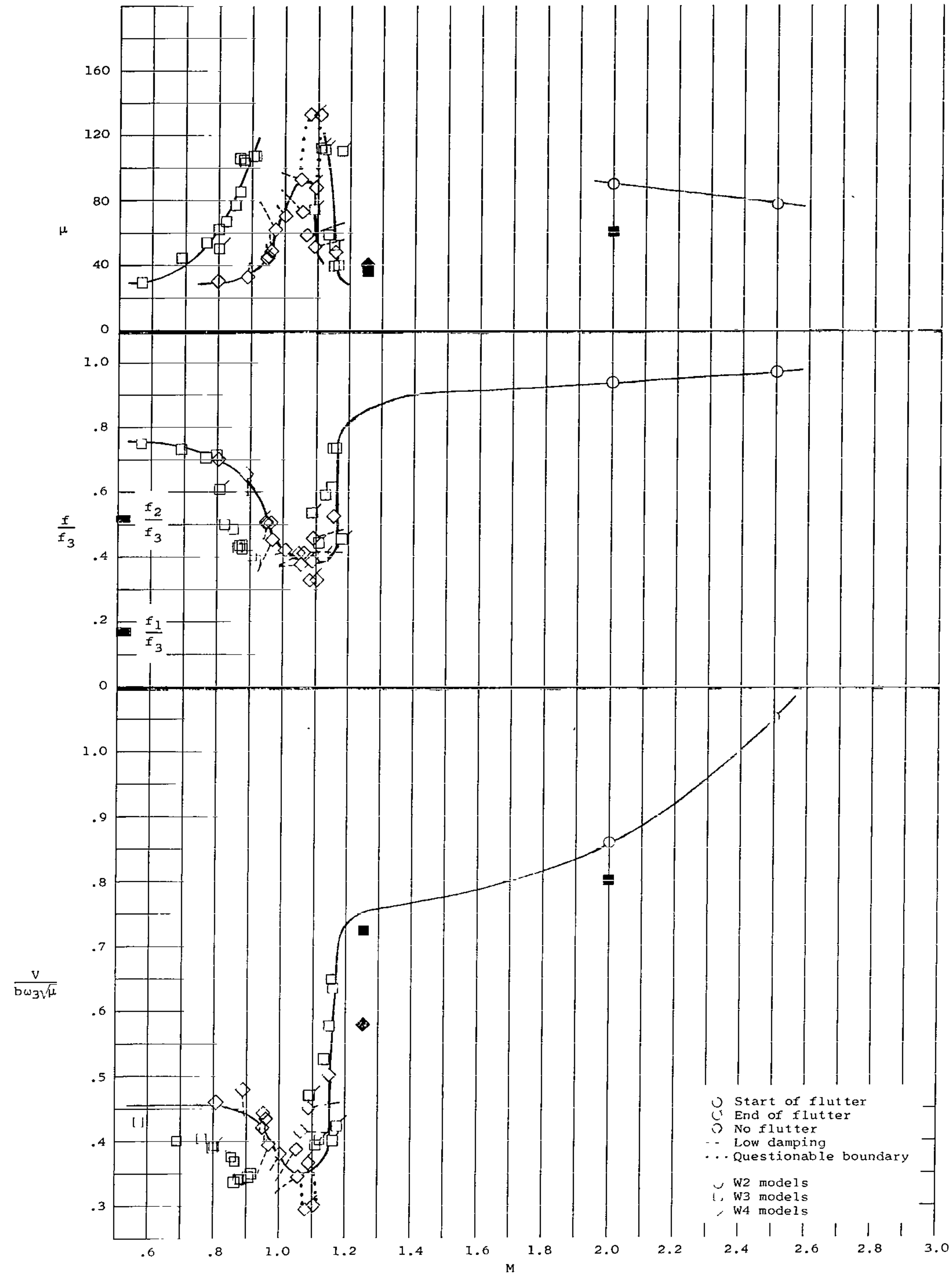

(b) Aspect-ratio-9 wing at $\Lambda = 39^{\circ}$.

Figure 4.- Continued.

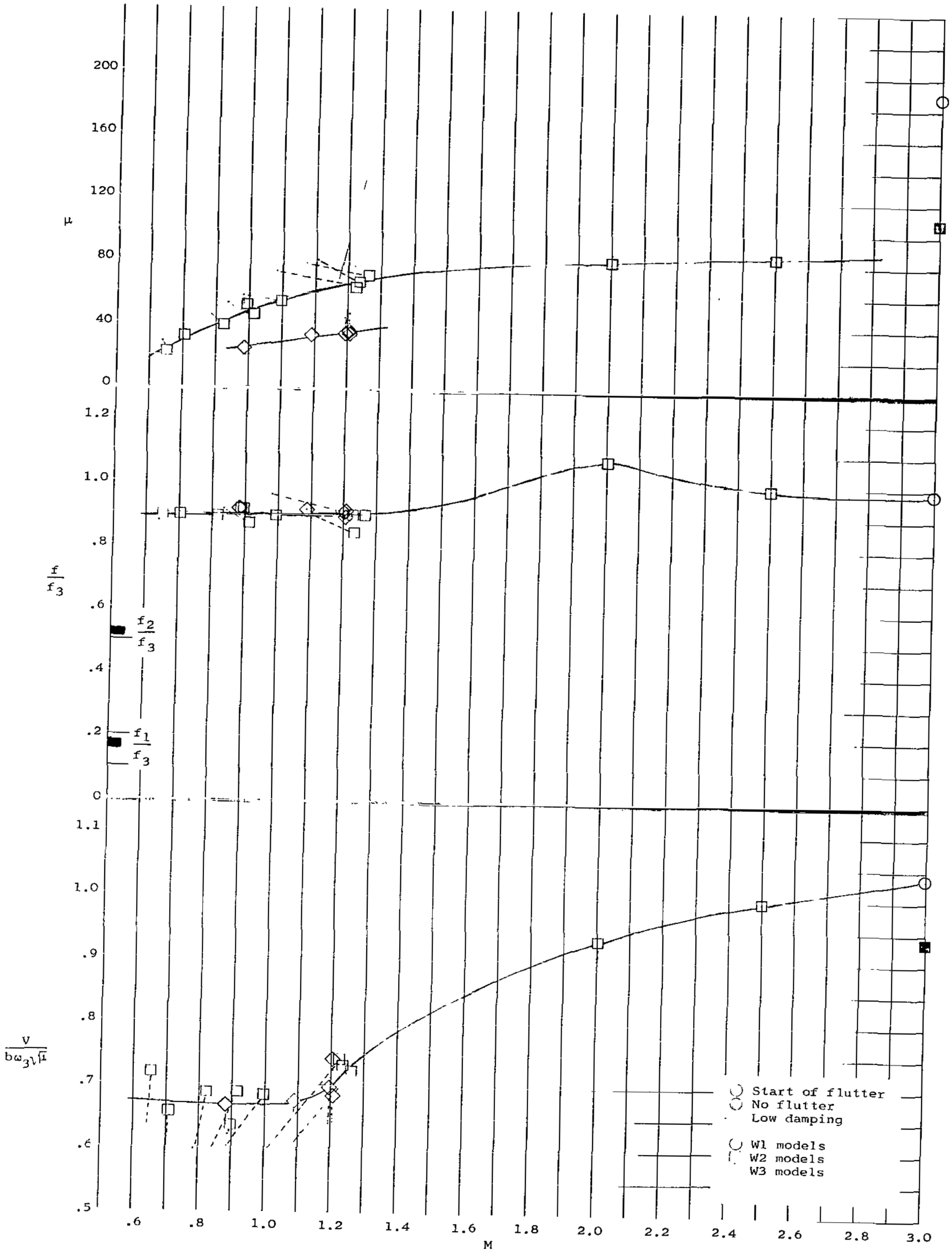

(c) Aspect-ratio-9 wing at $\Lambda = 73^{o}$.

Figure 4.- Continued.

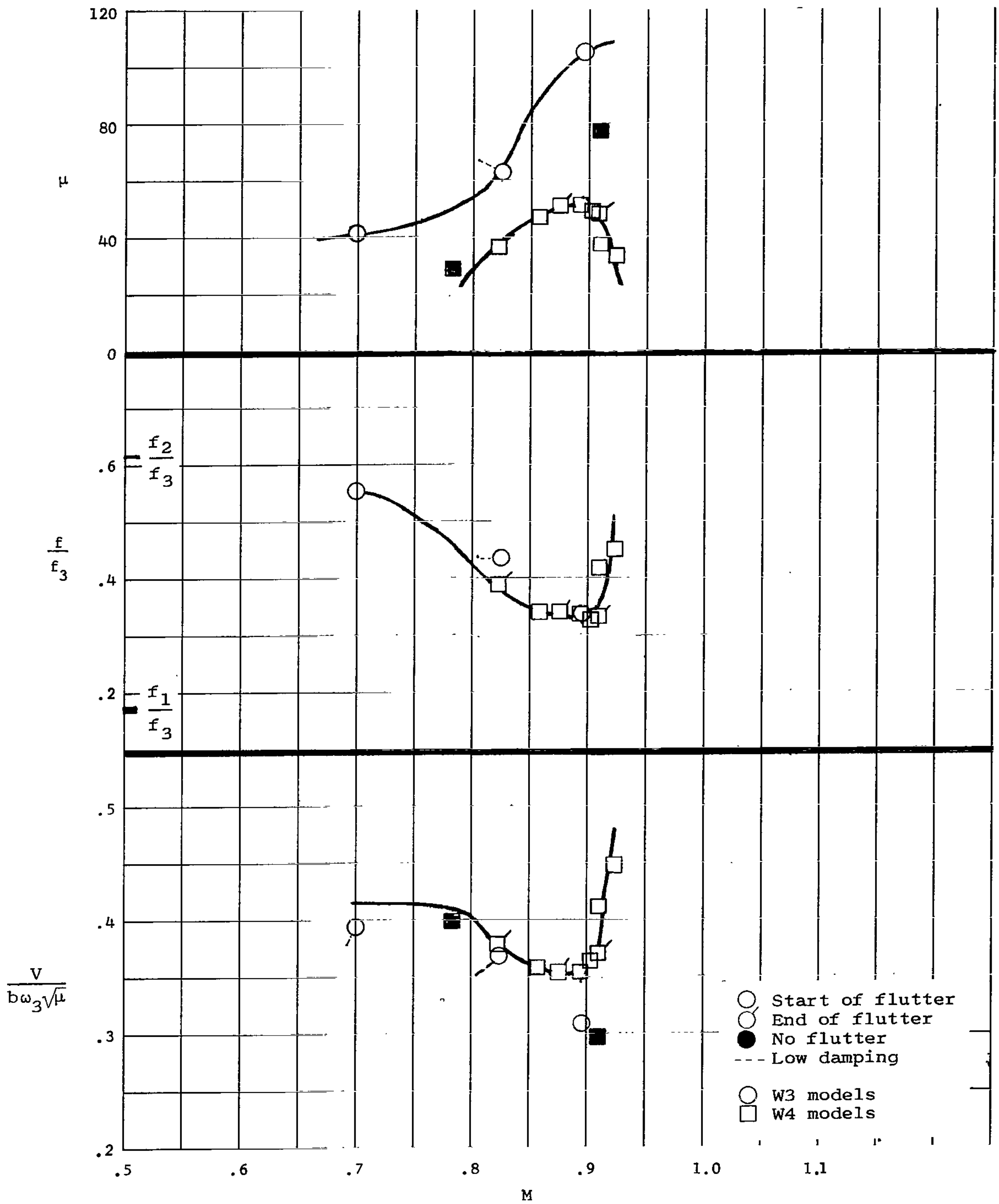

(d) Aspect-ratio-8 wing at $\Lambda = 16^0$.

Figure 4.- Concluded.

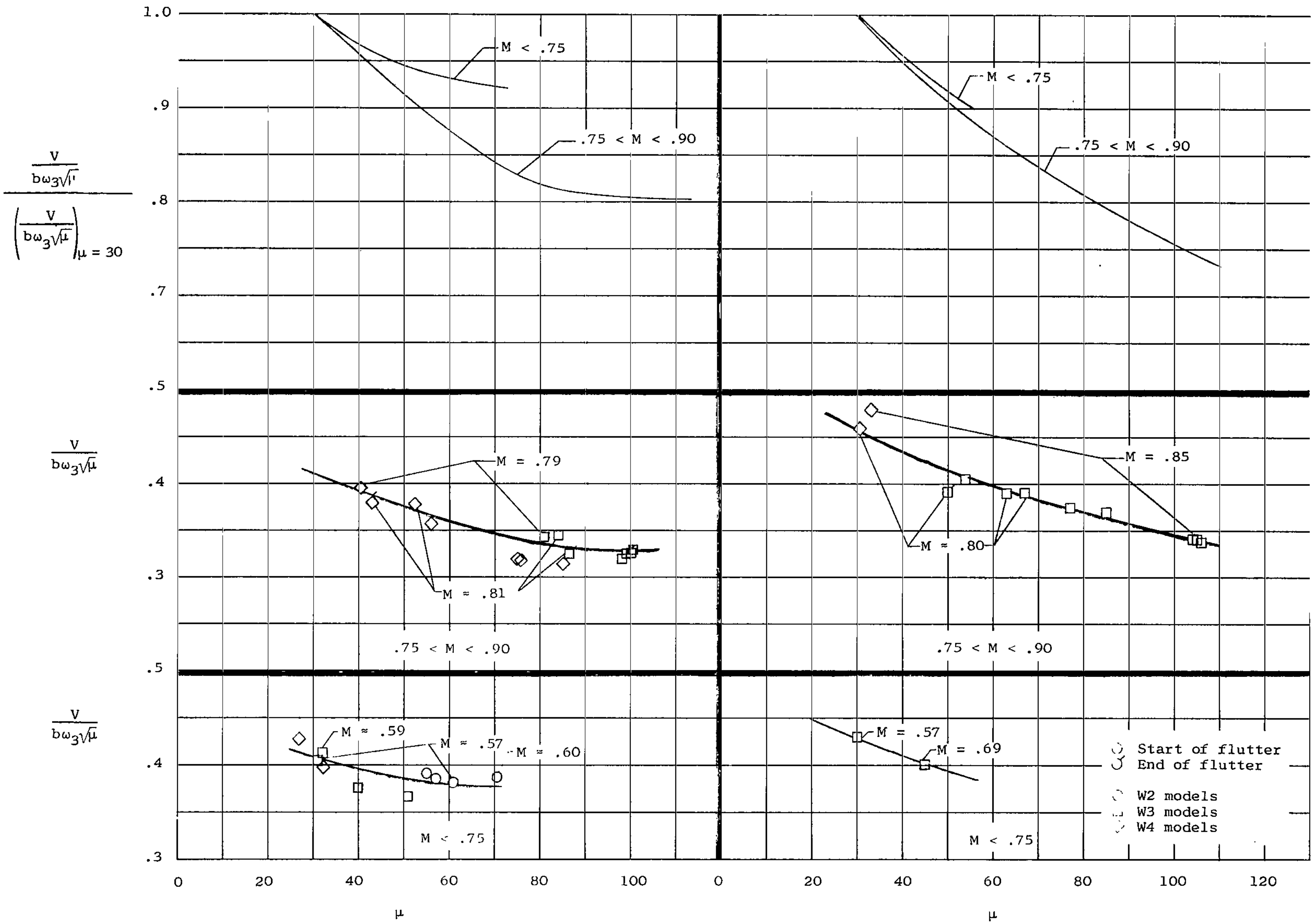

(a) $\Lambda = 16^{0}$.

(b) $\Lambda = 39^{0}$.

Figure 5.- Variations of flutter-speed index with mass-density ratio for the aspect-ratio-9 wing at $\Lambda = 16^{0}$ and $\Lambda = 39^{0}$ for Mach numbers up to 0.9.

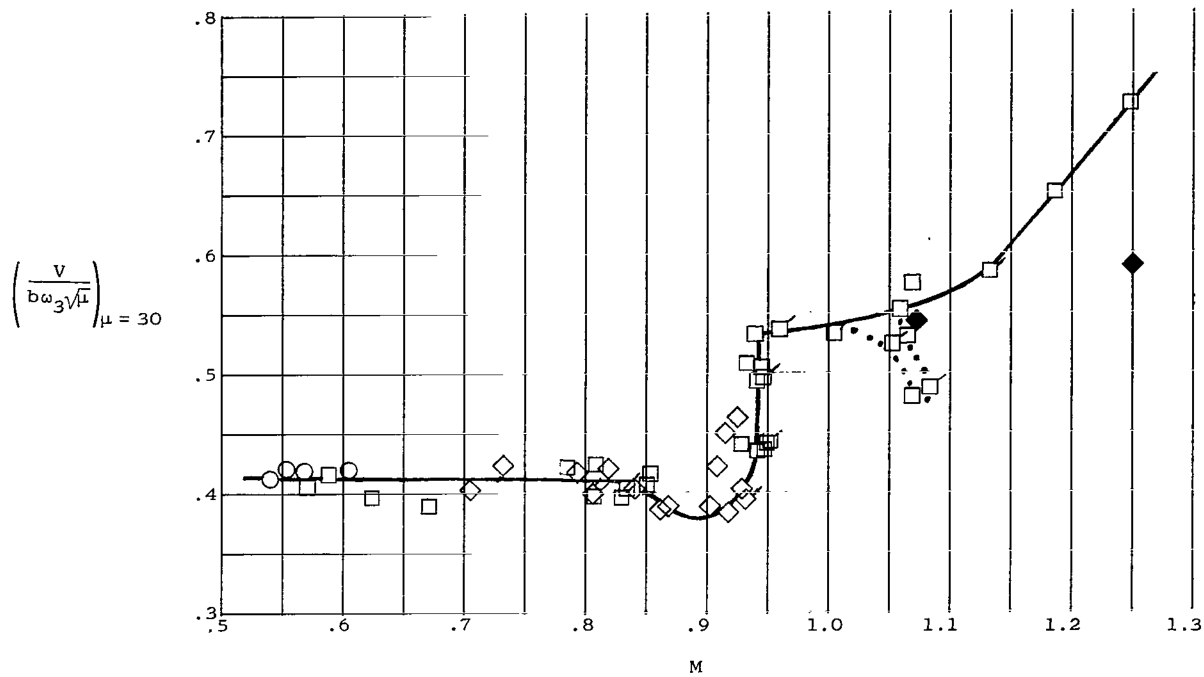

(a) $\Lambda = 16^0$.

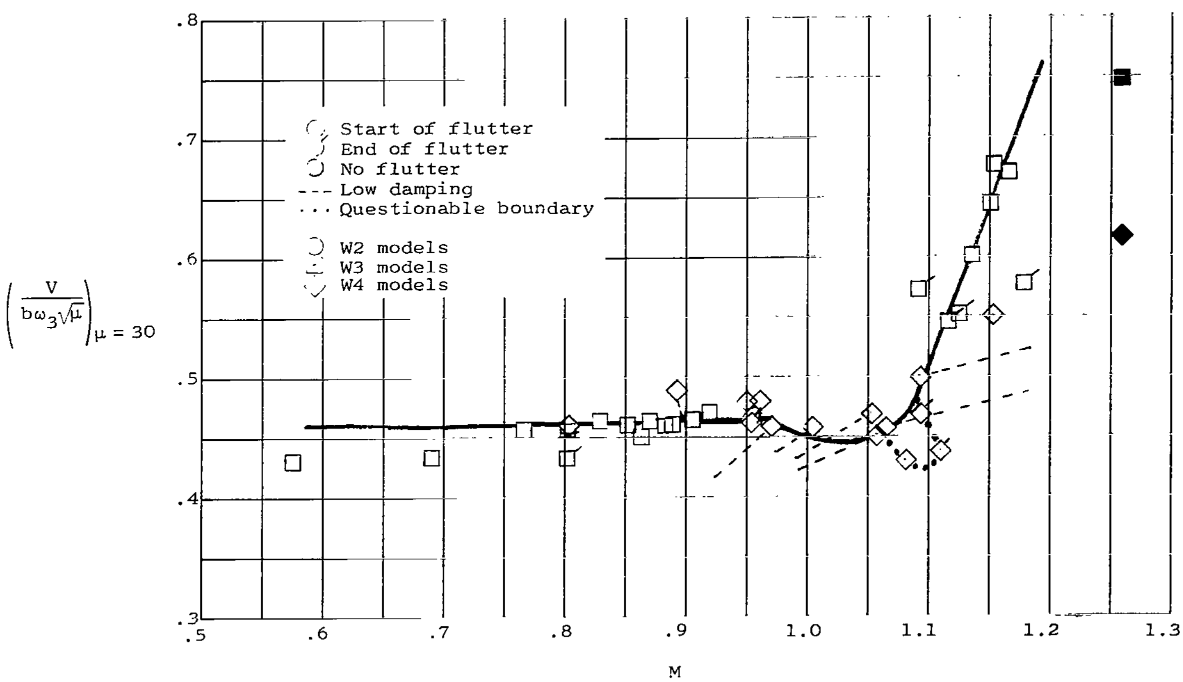

(b) $\Lambda = 39^0$.

Figure 6.- Variation with Mach number of flutter-speed index adjusted to a constant mass-density ratio (μ = 30) for aspect-ratio-9 wing at 16^0 and 39^0 sweepback angle.

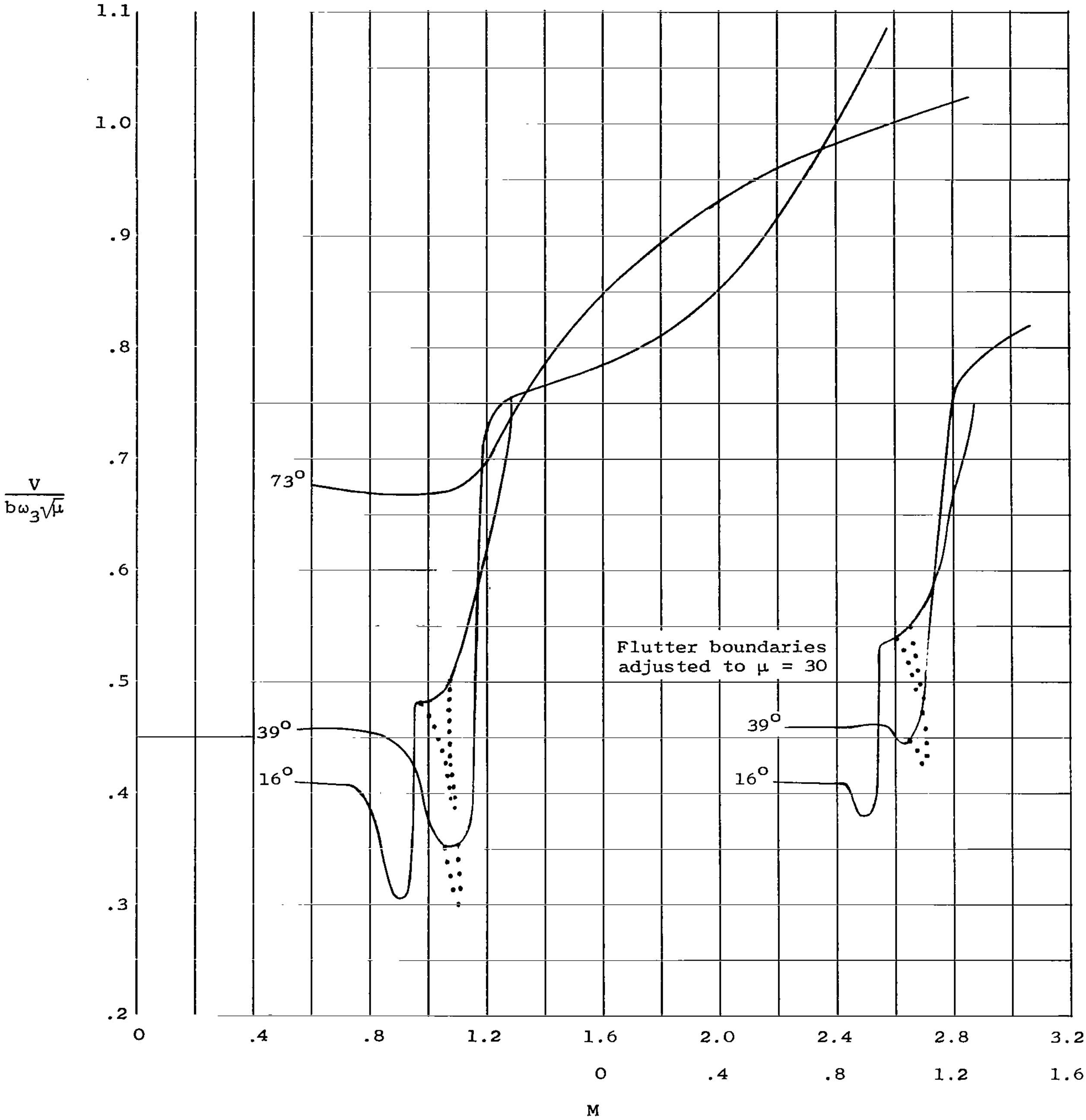

Figure 7.- The aspect-ratio-9-wing flutter boundaries demonstrating mass-density-ratio effects. (Dotted curves indicate questionable boundaries.)

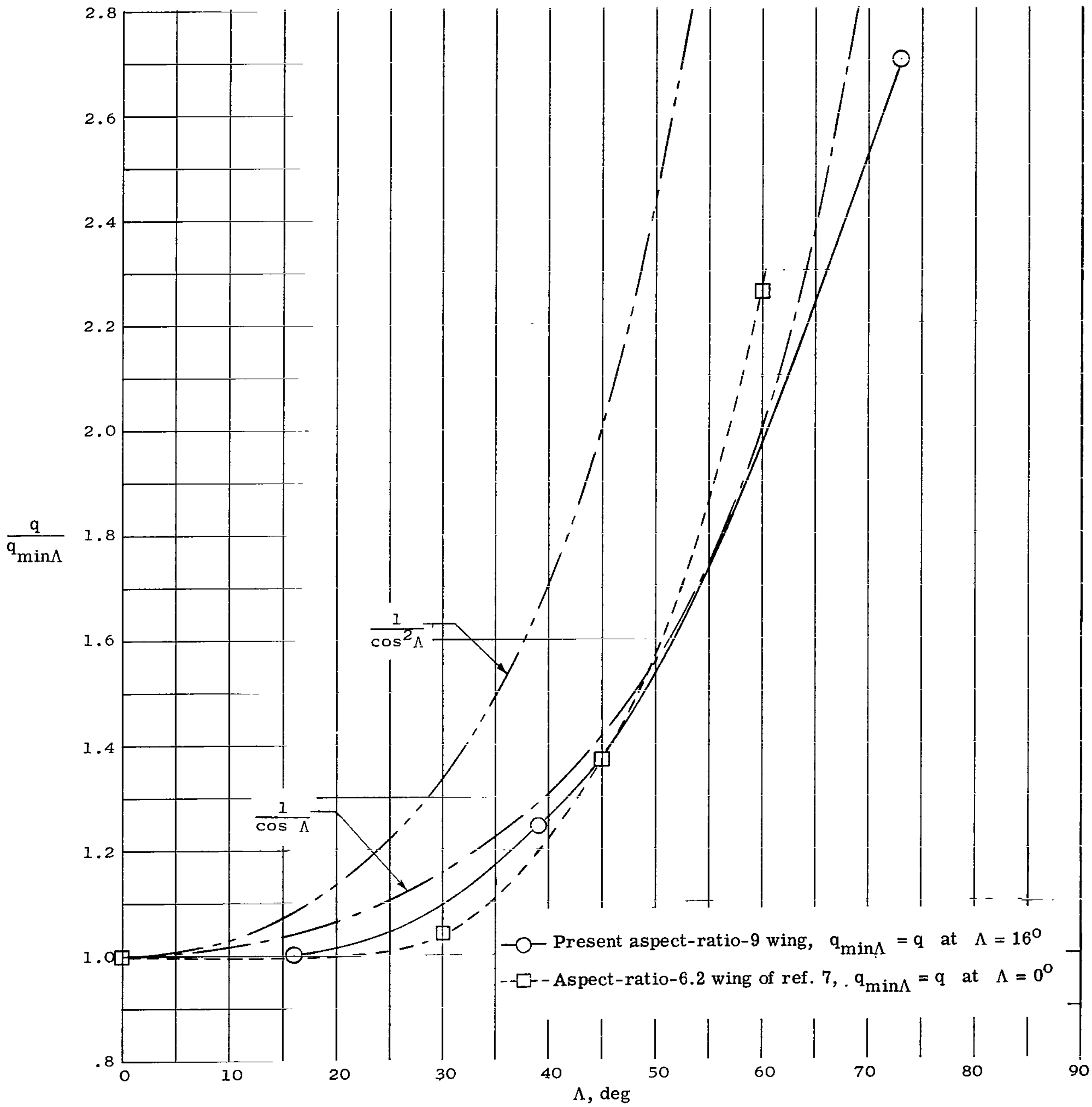

Figure 8.- Flutter dynamic-pressure ratio as a function of sweepback angle for experimental investigations using different models. $M \leq 0.6$.

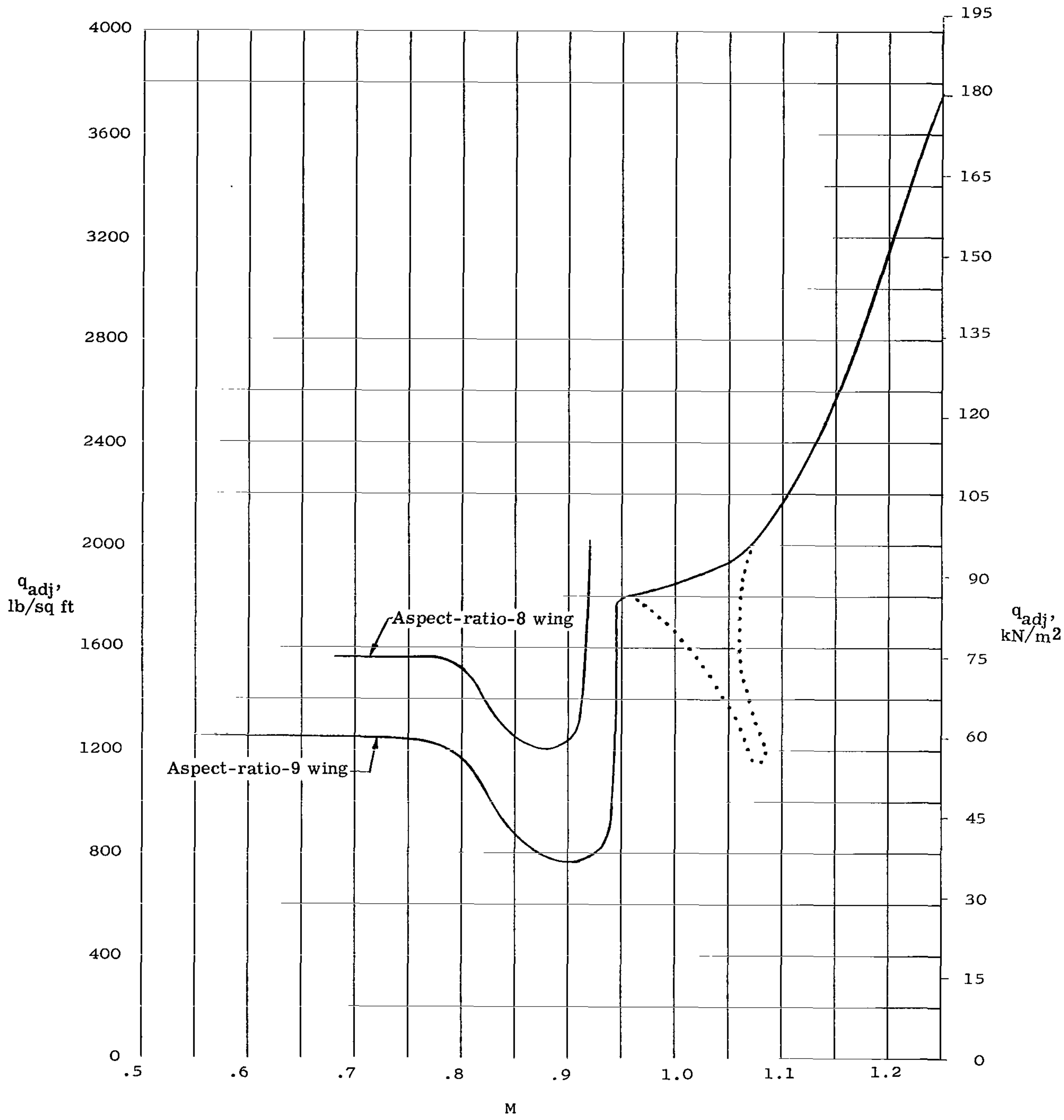

Figure 9.- Effects of aspect ratio on flutter dynamic pressure for 16° sweepback angle. (Dotted curve indicates questionable boundary.)

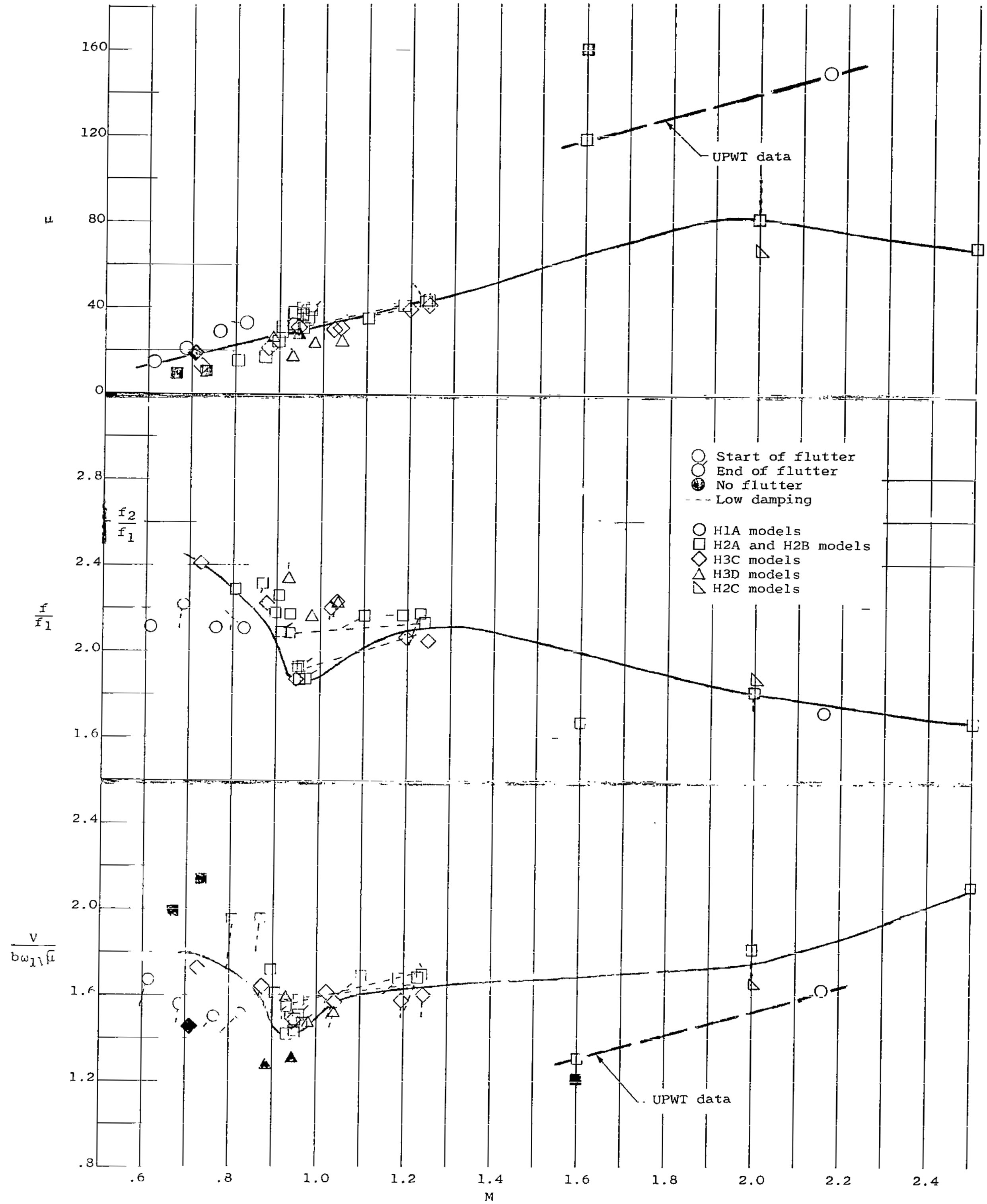

Figure 10.- Variation of flutter-speed index, flutter-frequency ratio, and mass-density ratio with Mach number for all-movable horizontal tail.

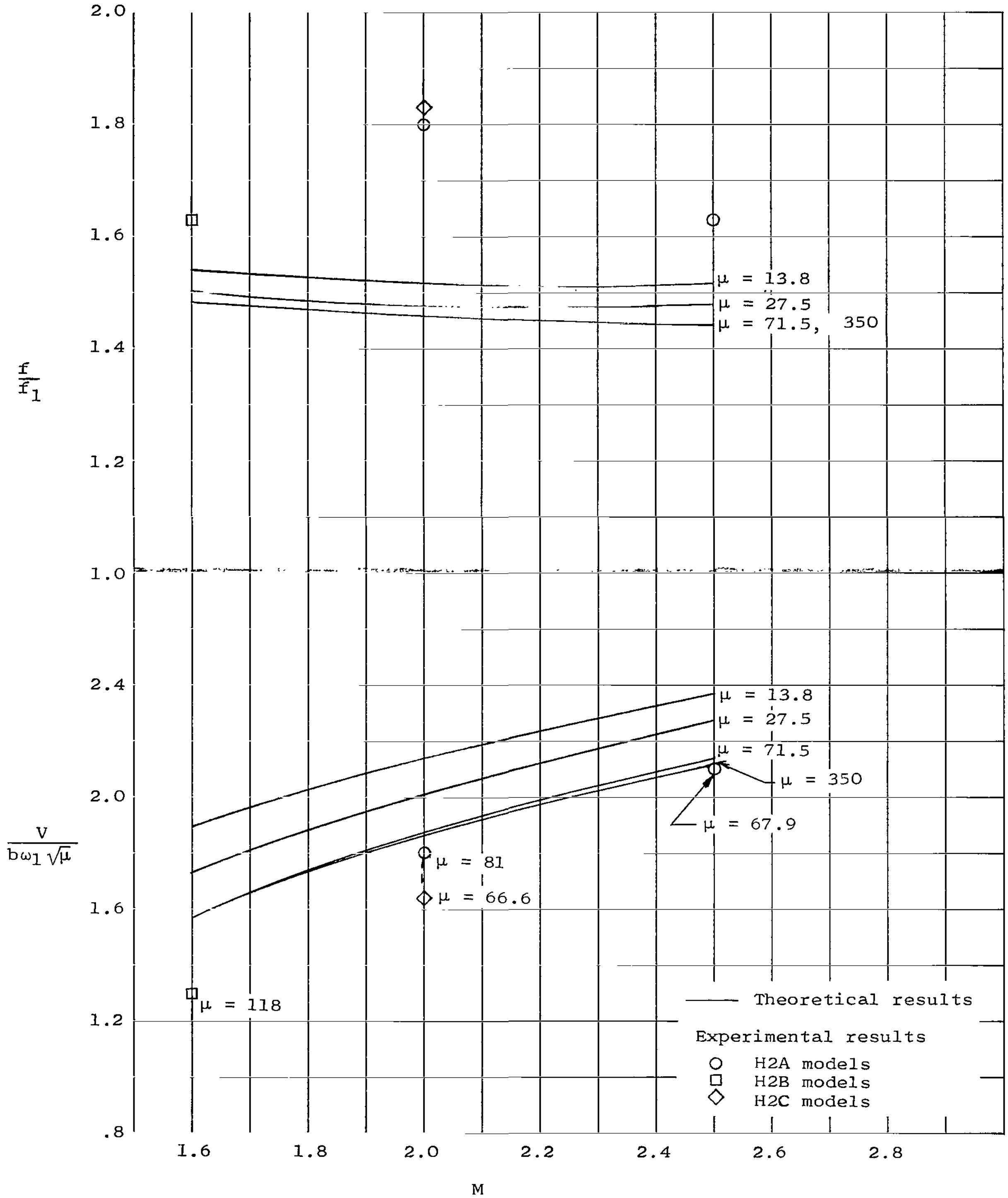

Figure 11.- Comparison of theoretical and experimental flutter results for horizontal tail H2 models at supersonic speeds.

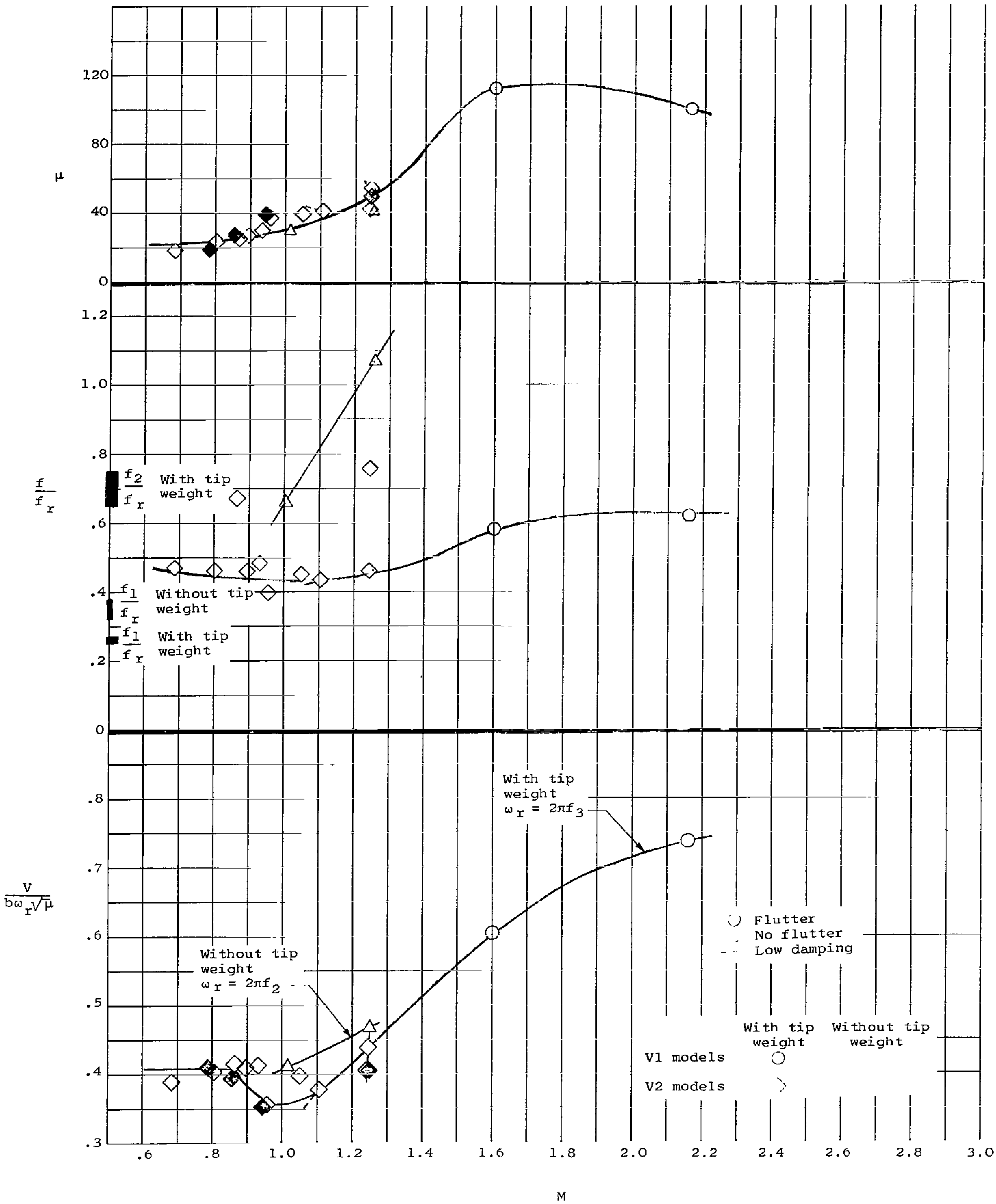

Figure 12.- Variation of flutter-speed index, flutter-frequency ratio, and mass-density ratio with Mach number for vertical tail with and without tip weight.

NASA-Langley, 1966 L-4831

"The aeronautical and space activities of the United States shall be conducted so as to contribute . . . to the expansion of human knowledge of phenomena in the atmosphere and space. The Administration shall provide for the widest practicable and appropriate dissemination of information concerning its activities and the results thereof."

—NATIONAL AERONAUTICS AND SPACE ACT OF 1958

NASA SCIENTIFIC AND TECHNICAL PUBLICATIONS

TECHNICAL REPORTS: Scientific and technical information considered important, complete, and a lasting contribution to existing knowledge.

TECHNICAL NOTES: Information less broad in scope but nevertheless of importance as a contribution to existing knowledge.

TECHNICAL MEMORANDUMS: Information receiving limited distribution because of preliminary data, security classification, or other reasons.

CONTRACTOR REPORTS: Technical information generated in connection with a NASA contract or grant and released under NASA auspices.

TECHNICAL TRANSLATIONS: Information published in a foreign language considered to merit NASA distribution in English.

TECHNICAL REPRINTS: Information derived from NASA activities and initially published in the form of journal articles.

SPECIAL PUBLICATIONS: Information derived from or of value to NASA activities but not necessarily reporting the results of individual NASA-programmed scientific efforts. Publications include conference proceedings, monographs, data compilations, handbooks, sourcebooks, and special bibliographies.

Details on the availability of these publications may be obtained from:

SCIENTIFIC AND TECHNICAL INFORMATION DIVISION

NATIONAL AERONAUTICS AND SPACE ADMINISTRATION

Washington, D.C. 20546